

***PBX 9501 High Explosive Violent Reaction:
Phase II Baseline and Aged Experiments***

Los Alamos
NATIONAL LABORATORY

*Los Alamos National Laboratory is operated by the University of California
for the United States Department of Energy under contract W-7405-ENG-36.*

Edited by Earlene Hammock, Comforce, Inc., for Group CIC-1
Photocomposition by Jan Dye, Group CIC-1

An Affirmative Action/Equal Opportunity Employer

This report was prepared as an account of work sponsored by an agency of the United States Government. Neither The Regents of the University of California, the United States Government nor any agency thereof, nor any of their employees, makes any warranty, express or implied, or assumes any legal liability or responsibility for the accuracy, completeness, or usefulness of any information, apparatus, product, or process disclosed, or represents that its use would not infringe privately owned rights. Reference herein to any specific commercial product, process, or service by trade name, trademark, manufacturer, or otherwise, does not necessarily constitute or imply its endorsement, recommendation, or favoring by The Regents of the University of California, the United States Government, or any agency thereof. The views and opinions of authors expressed herein do not necessarily state or reflect those of The Regents of the University of California, the United States Government, or any agency thereof. Los Alamos National Laboratory strongly supports academic freedom and a researcher's right to publish; as an institution, however, the Laboratory does not endorse the viewpoint of a publication or guarantee its technical correctness.

*PBX 9501 High Explosive Violent Reaction:
Phase II Baseline and Aged Experiments*

D. J. Idar

J. W. Straight

M. A. Osborn

C. B. Skidmore

D. S. Phillips

G. A. Buntain

PBX 9501 HIGH EXPLOSIVE VIOLENT REACTION: PHASE II BASELINE AND AGED EXPERIMENTS

by

D. J. Idar, J. W. Straight, M. A. Osborn, C. B. Skidmore,
D. S. Phillips, and G. A. Buntain

ABSTRACT

The Modified Steven test geometry was used to investigate the mechanical loading behavior and response of recently pressed (baseline) high explosive PBX 9501 and stockpile (aged) specimens. A 2 kg mild steel spigot projectile was launched via a powder-driven gun design, from approximately 37 to 103 m/s, at lightly confined PBX 9501 targets. Brief descriptions of the gun design and operation are given. The threshold velocity to reaction for various target designs and different PBX 9501 lots are reported. The violence of reaction, as measured by both passive and active techniques, is reported relative to a steady-state detonation in PBX 9501. Different diagnostics were employed to evaluate the impact timing and target strain behavior. Experimental results show delays to violent reactions as a function of projectile velocity, with decreasing delays as the velocity is increased. Posttest analyses of the PBX 9501 are briefly summarized. The experimental results show that the threshold to reaction for aged material does not differ significantly from the threshold for baseline material. The slight differences are postulated to be due to density variations.

INTRODUCTION

Low-velocity mechanical impact leading to unintentional reaction is of concern in accident scenarios involving the handling, transport, and storage of high explosives (HE). These have been investigated using different experimental techniques, from small- to large-scale, including, but not limited to the drop weight impact, Taylor anvil impact, Susan,¹ and more recently, the Steven and Modified Steven tests.²⁻⁷ Ideally, the data will be used to further advance 3-D computational predictive capability in chemistry-based reaction models for the assessment of HE response to mechanical insult.

The challenges in this type of research are numerous and complex. The HE formulations vary in composition, density, porosity, and particulate distributions. These differences directly affect the HE behavior and degree of sensitivity. Confinement and impactor characteristics also play a significant role in the behavioral response of the HE. Whether age plays a role in the response of the HE to this type of stimuli needs to be investigated.

It is important to note that determining the best method to extrapolate the data to different dimension and mass scales further complicates data interpretation and usefulness. The key is to determine which are the most relevant parameters leading to ignition/reaction with a sensitive, reproducible test configuration and reliable diagnostic measurements in tandem with computational analyses.

Our overall objectives for these experiments were to (1) evaluate the HE reaction threshold behavior for aged PBX 9501 relative to baseline, (2) characterize the degree of reaction violence relative to a detonation, (3) compare experimental results with past Modified Steven test data,⁶ and (4) provide data to continue development of a reliable 3-D computational predictive capability. This report summarizes our single impact test results with baseline and aged PBX 9501 in Modified Steven targets. The spigot gun design and operation are described. Threshold determinations, diagnostic details, timing, and relative reaction levels results are also described.

EXPERIMENTAL

Spigot gun design, mount, and characterization tests

Two kilogram, mild steel projectiles traveling at velocities between 37 and 103 m/s were used for these tests. For this purpose, a spigot gun, using rifle powder propellant, was designed to launch the projectile with the head external to the barrel and a shank extending inside the barrel. Three different barrel designs were used to cover the velocity range. Although similar, they differ in bore diameter, cartridge size, and barrel material. The internal barrel length was held constant at 6.75 in.

The first barrel design, with a 0.5-in. diameter bore and 2.0-in. outer diameter (o.d.) used a standard .45-.70 rifle cartridge to contain the primer and powder. The muzzle was designed with four ports to vent the powder combustion gases and reduce projectile tip-off at exit. The projectile was constructed with a 0.5-in. diameter spigot, 6.25-in. long with a 3.0-in. diameter hemispherical head. A 0.5-in. long, polyethylene obturator was used to seal the powder gases. This worked well at low velocities, but the spigot shank buckled in the barrel at higher velocities.

The second barrel design required a simple modification of the barrel, and changes in the spigot and obturator. The bore was increased to 0.75-in. diameter, the spigot was shortened to 5.25-in., and the obturator was lengthened to 1.5 in. Velocities ranging from 24.5 to 94.6 m/s were obtained in 142 different tests using this design. At velocities greater than 64.0 m/s, the higher pressures expanded the base of the spigot causing excessive friction in the barrel. This problem was mitigated by tapering the end of the shank by 0.01-in., allowing velocities up to 76.2 m/s. Higher velocities required shanks of A-1 tool steel hardened to Rc-51. At velocities greater than 82.3 m/s, the pressures were high enough to cause low-cycle fatigue with attendant barrel ruptures.

The third barrel was constructed from American Iron and Steel Institute 4340 steel heat-treated to Rc-37 with the barrel o.d. increased to 3 in., and the same diameter bore as the second barrel. The longer .45 basic cartridge was used with this barrel design to contain a larger powder load. The breech/receiver o.d. was also increased to mate to the larger barrel

o.d. The projectile and obturator design remained the same as for the second barrel. Forty-three tests have been conducted using this design with velocities between 73.5 and 109.5 m/s.

The large mass of the projectile causes the powder to burn almost as if it were in a closed container. The combined powder curves for the 2.0- and 3.0-in. o.d. barrels are shown in Figure 1. As with any powder gun, certain loads produce more velocity scatter than others. The data do not follow the same curve as a result of the different cartridges used. Burn pressures were measured first with piezoelectric pressure transducers and then with strain gauges. The high pressures saturated the 100 ksi transducers, and occasionally blew them out of the barrel. Subsequently, both hoop and axial strain gauges were used, and pressures as high as 161 ksi have been measured in the chamber. Examples of the strain measurements and computed pressure are shown in Figures 2 and 3.

A gun barrel is neither an ideal closed cylinder nor an open one. One might expect the axial strain measurement to lie between these two conditions, but as can be seen in Figure 2, this is clearly not the case. The strain starts out negative (compressive) and then oscillates at high amplitude. The initial compression is due to the Poisson effect combined with the undefined end conditions of the barrel. The initial contractions of the material then excite the axial natural frequencies of the barrel. This explanation was verified by comparing a fast Fourier transform (FFT) analysis of the strain data with a finite element analysis of the gun. The frequencies present in the data match the computed axial natural frequencies of the gun assembly.

The extremely violent recoil of the gun requires a massive sliding gun mount to provide reproducible impact points. The impact point is a function of powder load, but is quite consistent for a given load. Tests are performed with plywood (inert) targets to verify both velocity and impact point before each live target test. For safety reasons, the gun is remotely operated with an electrically actuated, pneumatically driven firing mechanism. Further details of the gun design, the powder loads, and the velocities may be found in Reference 6, a report on the first series of experiments.

Target designs

The basic target design started as a modification of the target assembly used in the original target series⁶ and those used by Chidester et al. with HE and target material constraints in mind. The design, as depicted in Figure 4 and defined in Table 1, consisted of a holder, cover plate, and retaining ring. The PBX 9501 article was centered and covered with a 0.020-in. thick Sylgard 184 layer and the cover plate. The design allowed for an annular gap of 0.125-in. between the HE o.d. and the holder inner diameter (i.d.). The targets were assembled and secured to a mild steel backing plate, 12.0-in. square by 3.0-in. thick with a 0.75-in. deep cavity, which served as a high-impedance boundary.

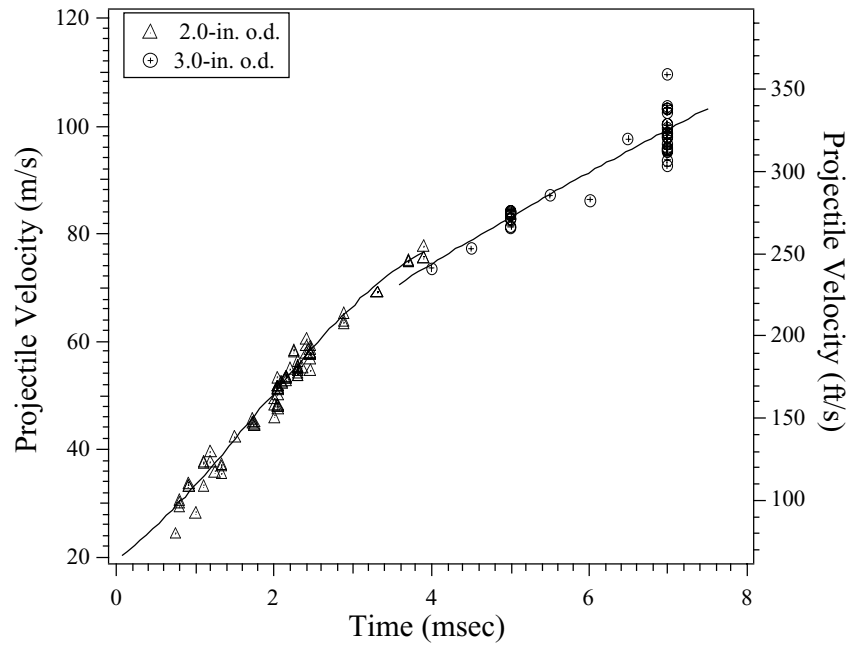


Figure 1. Powder curves.

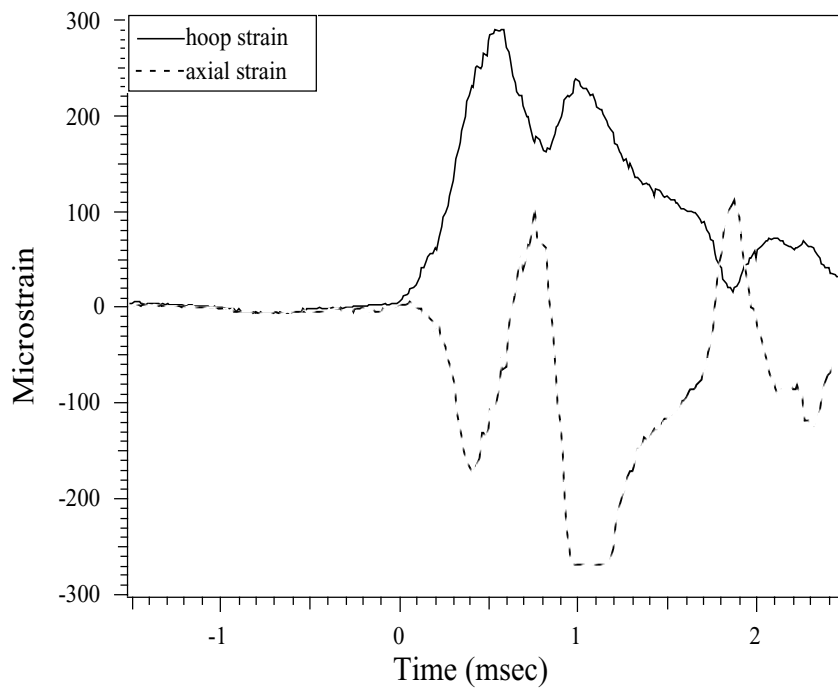


Figure 2. Hoop and axial strain measurements obtained from the high-pressure barrel design.

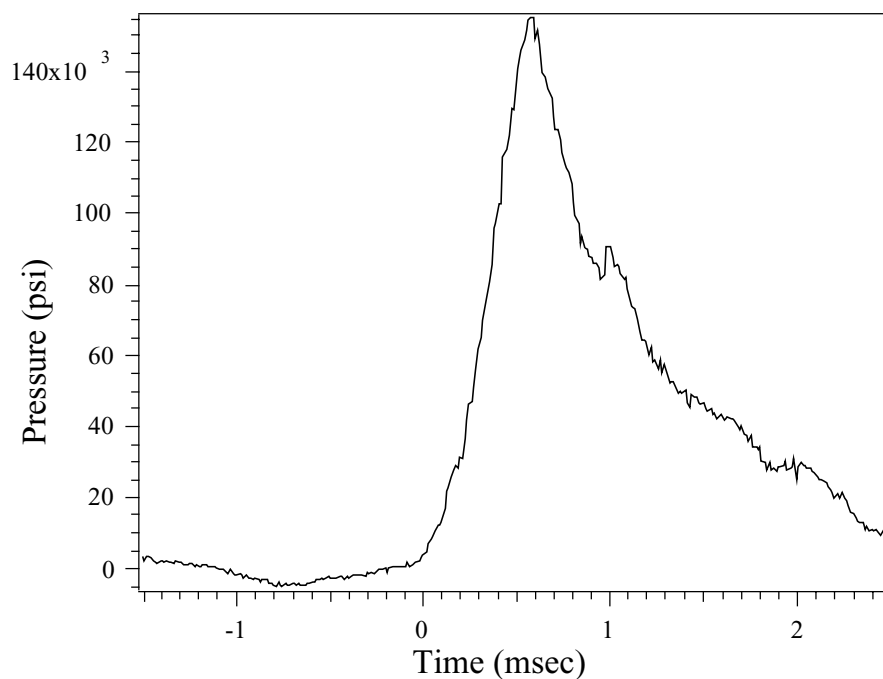


Figure 3. Bore pressure as a function of time for the high-pressure barrel.

PBX 9501 sample/specimen history

Three different lots of PBX 9501 were used in these tests. PBX 9501 is a conventional high explosive (CHE) formulation composed of 94.9/2.5/2.5/0.1 wt % of HMX, Estane 5703, a eutectic mixture of bis(2,2-dinitropropyl)acetal and bis(2,2-dinitropropyl)formal (abbreviated as either BDNPA-F or NP for nitroplasticizer), and a stabilizer/free radical inhibitor (either diphenylamine [DPA] or Irganox 1010). The HMX in PBX 9501 is composed of a three-to-one ratio of coarse-to-fine grades of HMX. The Estane 5703 is an amorphous, thermoplastic polyester polyurethane with a glass transition temperature (T_g) of -31°C .⁸ The addition of the BDNPA-F plasticizer causes the polymer strength to decrease, but the toughness and flexibility are increased. The plasticizer acts as a lubricant to promote the sliding of the polymer chains, and to reduce the degree of entanglement. The stabilizer/inhibitor reduces free radical reactions and mitigates molecular weight degradation of the Estane 5703.

The lot numbers, formulation year, average densities, and compositional analyses for the three library lots are given in Tables 2 and 3. The lots differ in formulation age, density, and in composition. The oldest lot tested, 685-002, was stabilized with diphenylamine and the other two with Irganox 1010. Lot 730-010, the youngest, still meets the PBX 9501 molding powder specifications, and was defined as the baseline lot for these tests. A comparison of the compositional analyses and Estane molecular weights shows that lot 685-002 has the highest weight percentage of HMX and RDX and the lowest molecular weight values for the Estane 5703.

The baseline PBX 9501 specimens were machined from samples pressed in 1997 and 1998. Aged specimens were obtained from W76 Stockpile Laboratory Test (SLT) hemishells produced from lots 685-002 and 730-005. These were pressed in the late 1970s and early 1980s. The aged material was also denser than the baseline specimens. The aged specimens were installed in the targets to insure consistent orientation with the prior SLT orientation in mind. All of the specimens were machined to 5.0-in. diameter by 0.5-in. thick.

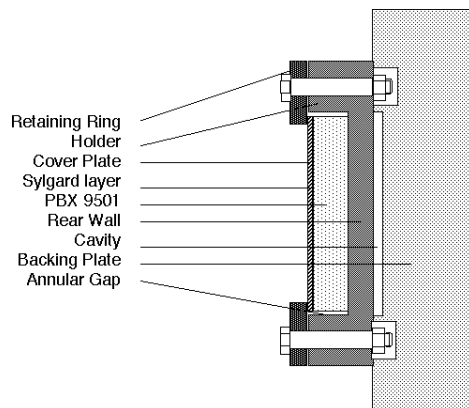


Figure 4. Basic Modified Steven target.

Table 1. Target design materials and dimensions

Design	Cover Plate	Holder	Retaining Ring
Small, thin	304 stainless steel	A36 steel	A36 steel
	0.118 \pm 0.001-in. thick	5.250 \pm 0.005-in. i.d.	4.500 \pm 0.005-in. i.d.
	5.000 \pm 0.005-in. diameter	7.500 \pm 0.005-in. o.d.	7.500 \pm 0.005-in. o.d.
		0.638 \pm 0.002-in. deep	0.500 \pm 0.002-in. thick
		0.750 \pm 0.005-in. thick rear wall	

Table 2. PBX 9501 specimen data

Lot #	Formulation Year	Average Immersion Density (g/cm ³)	Library Lot Estane M _w ^a	Library Lot Estane M _p ^a	Library Lot Estane M _n ^a
685-002	1977	1.840	87093 \pm 672	85583 \pm 1296	54783 \pm 129
Aged					
730-005	1981	1.840	102553 \pm 991	94841 \pm 1200	65372 \pm 291
Aged					
730-010	1989	1.830	107665 \pm 1001	97762 \pm 1239	68284 \pm 187
Baseline					

^aThe Estane 5703 molecular weight data were determined using gel permeation chromatography (GPC) relative to a polystyrene standard in tetrahydrofuran solution on the library lot specimens. The library lot specimens were stored as molding powder, bagged in approximately 50 lb boxes in magazines at the Pantex Plant, Amarillo, Texas. Specimens were shipped to Los Alamos National Laboratory (LANL) for compositional and GPC analyses.

Table 3. PBX 9501 library lot composition data

Component	Lot 685-002		Lot 730-005		Lot 730-010	
	Wt %		Wt %		Wt %	
HMX	95.0704 ±	0.1094	94.6925 ±	0.0017	94.8172 ±	0.0641
RDX	0.2388 ±	0.0274	0.0449 ±	0.0003	0.0006 ±	0.0001
Estane	2.4535 ±	0.0107	2.4566 ±	0.0193	2.4342 ±	0.0192
BDNPF	0.9969 ±	0.0330	1.3568 ±	0.0056	1.2000 ±	0.0782
BDNPA	1.1041 ±	0.0352	1.4140 ±	0.0073	1.1630 ±	0.0687
Stabilizer ^a	0.0597 ±	0.0014	0.0535 ±	0.0002	0.0695 ±	0.0065
PBNA	0.00331 ±	0.00011	0.00348 ±	0.00001	0.00330 ±	0.00026

^aLot 685-002 is stabilized with DPA and Lots 730-005 and 730-010 are stabilized with Irganox 1010.

Diagnostics

A cheap, easily replaceable light box/photodiode system was designed for determining the projectile velocity. Three halogen lights, each with a corresponding photodiode, were spaced at three-inch intervals in a wooden frame for this purpose. The data records yield three light profiles producing two independent velocity measurements.

A polyvinylidene fluoride (PVDF) gauge was attached to the front surface of the target to record the projectile impact time. The gauges have proved to be reliable, but are quite noisy and can cause interference on other diagnostic records. The impact timing provides an additional data point to evaluate the projectile velocity. This datum is averaged with the velocity data from the photodiode box.

One to two strain gauges were mounted on center of the target's rear surface to record the deformation relative to the time of impact. If two strain gauges were used, they were oriented with their elements at right angles to each other. MicroMeasurements EA-06-500BH-120 strain gauges amplified with Vishay model 2311 signal conditioners were used for this purpose. Several iterations of gauge and lead wire mounting schemes were used to increase data collection time. The gauges and lead wires typically survived after the projectile impact and rebound. Data loss occurred when the gauges were either crushed between the back plate and the rear mounting block or when the cables were destroyed.

Violence of reaction/delay to reaction

Predicting the degree of violence of PBX 9501 reactions for a given reaction is desirable for risk assessments and a goal for computational models. A ballistic pendulum and blast overpressure gauges were used to determine the violence of reaction relative to a PBX 9501 steady-state detonation. The two entirely different methods produced strikingly similar results, not only for high levels of reaction, but also for very low levels of reaction. The classic ballistic pendulum designed at LANL is shown in Figure 5. The pendulum weight was adjusted to 2098 lb for the small targets by adding or removing 95 lb plates from the pendulum box. The mild steel backing plate added approximately another 110 lb to the overall weight. Momentum transfer calculations were performed for varying amounts of detonating PBX 9501 for two different pendulum weights. These were benchmarked with four PBX 9501 calibration charges. The degree of pendulum displacement was measured using two independent passive measurements: a friction pivot-arm that locks in place at the

peak of the pendulum swing, and a thin cable, labeled with a marker, displaced by the pendulum swing. Tests that did not result in a violent reaction of the HE were described as quenched and/or damaged.



Figure 5. Ballistic pendulum with a PBX 9501 calibration target attached.

The blast overpressure gauge data were obtained with two PCB Piezotronics, Inc. Model 102A15 transducers, 0–200 psi, in face-on mode positioned at 45° off of the projectile axis, at a distance of 10 ft from the front target face. Power to the transducers was provided by a PCB Piezotronics power supply. Output signals were coupled at 1-M Ω AC into LeCroy 9400A oscilloscopes. Pressure and timing calibrations were accomplished in tandem with the ballistic pendulum calibration tests. The blast gauge measurements were averaged with the ballistic pendulum data to determine an average energy release relative to a full detonation. The time interval between impact and violent reaction was estimated with two methods. The delay time was estimated from strain gauge records, and/or by comparison of the impact and blast wave timing.

POSTTEST TARGET CHARACTERIZATION

The posttest characterization methods can be categorized into nonintrusive and intrusive techniques. Only a brief summary of the techniques will be provided here. Phillips, and Skidmore, et al.^{9,10} have described these techniques and their results in more detail.

Nonintrusive techniques included dent/deformation measurements, visual examination of the PBX 9501 surface, and radiographs of the cracked PBX 9501. The dent data were used to evaluate the material models for the engineering codes. The front dent data were analyzed from depth measurements obtained from the top-to-bottom and left-to-right axes on the front surface of the cover plates or the inside surface of the target assembly. These depth data are provided in detail for each target in the appendix. Typically, if impact did not occur on center, the front dent data were measured twice, once through the impact (IMPACT) point, and once through the center (CENTER) face of the target. Any exceptions are in the appendix. The average measured dent depths for the targets are given in Table 4.

Table 4. Target projectile velocities, impact point, and average measured dent depths

Test #	Projectile Velocity (m/s)	Impact Point	Average Measured Dent Depth on Cover Plate (mm)	Average Measured Dent Depth on Inside Surface of Holder (mm)
K8-2147	36.9 ±0.8	On center left-to-right, 0.1875-in. high	8.26 ±0.02	
K8-2150	49.4 ±1.1	0.375-in. left, 0.125-in. high	11.26 ±0.03	
K8-2168	51.8 ±1.2	0.125-in. right, 0.1875-in. high	11.89 ±0.19	
K8-2165	52.7 ±1.2	0.375-in. right, 0.50-in. high	12.37 ±0.08	
K8-2174	54.4 ±1.3	0.5-in. left, 0.5-in. low	10.99 ±0.37 ^a	
K8-2171	55.9 ±1.3	0.1875-in. left, 0.1875-in. high		0.25 ±0.10
K8-2162	57.9 ±1.3	0.50-in. right, 0.50-in. high		0.24 ±0.01
K8-2159	68.9 ±1.6	0.25-in. left, on center high to low		0.75 ±0.02
K8-2156	74.4 ±1.7	0.5-in. right, 0.1875-in. high		1.88 ±0.09
K8-2153	77.7 ±1.8	0.25-in. right, 0.375-in. high		2.46 ±0.26
K8-2178	45.0 ±1.0	0.375-in. left, 0.25-in. low	10.32 ±0.16	
K8-2300	48.0 ±1.1	0.4375-in. right, 0.5-in. high	10.44 ±0.03	
K8-2180	51.8 ±1.2	0.125-in. right, on center high to low	11.88 ±0.01	
K8-2183	53.0 ±1.2	0.5-in. left, 0.125-in. high		0.15 ±0.01
K8-2176	54.3 ±1.2	0.125-in. right, and 0.125-in. high		1.51 ±0.08
K8-2297	54.4 ±1.3	0.125-in. right, 0.125-in. high		0.27 ±0.17
K8-2303	55.1 ±1.3	On center		0.30 ±0.01
K8-2306	103.0 ±2.4	On center left-to-right, 0.25-in. high		6.09 ±0.11

^aThe dent measurement on the stainless steel cover plate of test K8-2174 was obtained after the cover was removed from the target.

Visual examination of the HE top surfaces verified that the PBX 9501 (1) had expanded to fill the annular gap, and (2) displayed radial cracks emanating from the impact point, with some evidence of shear dislocation. Examples of this can be seen in the images of the first target, K8-2147 as shown in Figure 6 (see the appendix for more images of the targets). High-energy x-rays, 2.2 MeV, were used to obtain posttest radiographs (see the appendix) of the damaged and quenched targets. Targets were radiated for approximately 1 minute at 2.2 MeV using a film/screen stack consisting of the following 5 layers: (1) 0.010-in. thick lead, (2) M file, (3) 0.003-in. thick lead, (4) M film, and (5) 0.010-in. thick lead. The radiographs were digitized and enhanced with numerical methods to further evaluate the crack variations in the HE after impact.

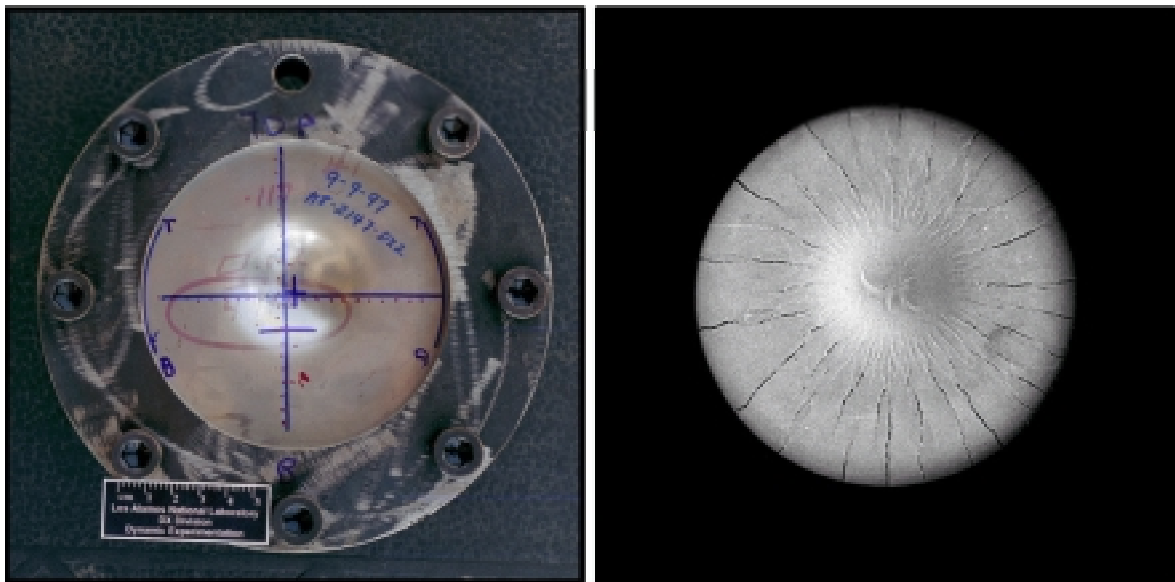


Figure 6. Images of target K8-2147 with and without the cover plate showing the front dent and crack damage to the PBX 9501 after a 36.9 m/s impact.

Figure 7 shows images of the K8-2147 radiographs before and after numerical enhancement. The dark center on the enhanced image is produced as an artifact of the numerical enhancement method. Extensive posttest characterization was also performed on the PBX 9501 recovered from the fifth target K8-2174, impacted at 54.4 m/s, just below threshold velocity. Regions of the target where some level of reaction was indicated by fissures or cracks were the focus of the characterization. The principal techniques employed were polarized light microscopy (PLM) and scanning electron microscopy (SEM). That evaluation suggested the presence of re-solidified melt and other phases of HMX. Reflectance Fourier transform infrared (FTIR) spectroscopy, second harmonic generation (SHG),¹¹ and powder x-ray diffraction were used to confirm the presence of delta HMX.

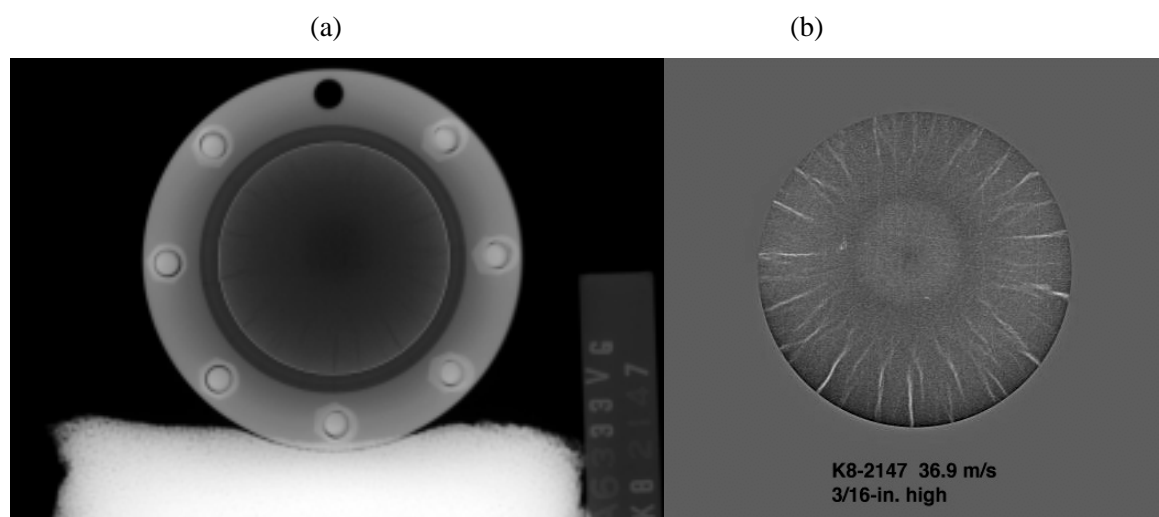


Figure 7 (a–b). (a) Digital image of target K8-2147 radiograph. (b) Numerically enhanced digital image of the inner diameter of target K8-2147. The diameter of the image in figure (b) is equal to the innermost diameter in figure (a).

Two regions were sampled for PLM and SEM analysis. One was just under the impact point of the nose of the projectile. Here, there were indications of melt on the surface against the metal holder and just under the front HE surface. Dissection of the nose region revealed a path that connected with the principal fissure (radial). PLM analysis of the fissure region had similar indications that melt had occurred.

Figure 8 shows a typical melt region in cross-section. Three layers are apparent. The top layer is of uniform contrast and appears to contain many facsimiles of bubbles, presumably formed by the evolution of decomposition gases while the melt was solidifying. The second layer is characterized by highly textured contrast in the region of a parent crystal nearest the first layer. This is indicative of a transition region between that which was melted and that which was not. The third layer, or parent material, resembles only mechanically damaged material.

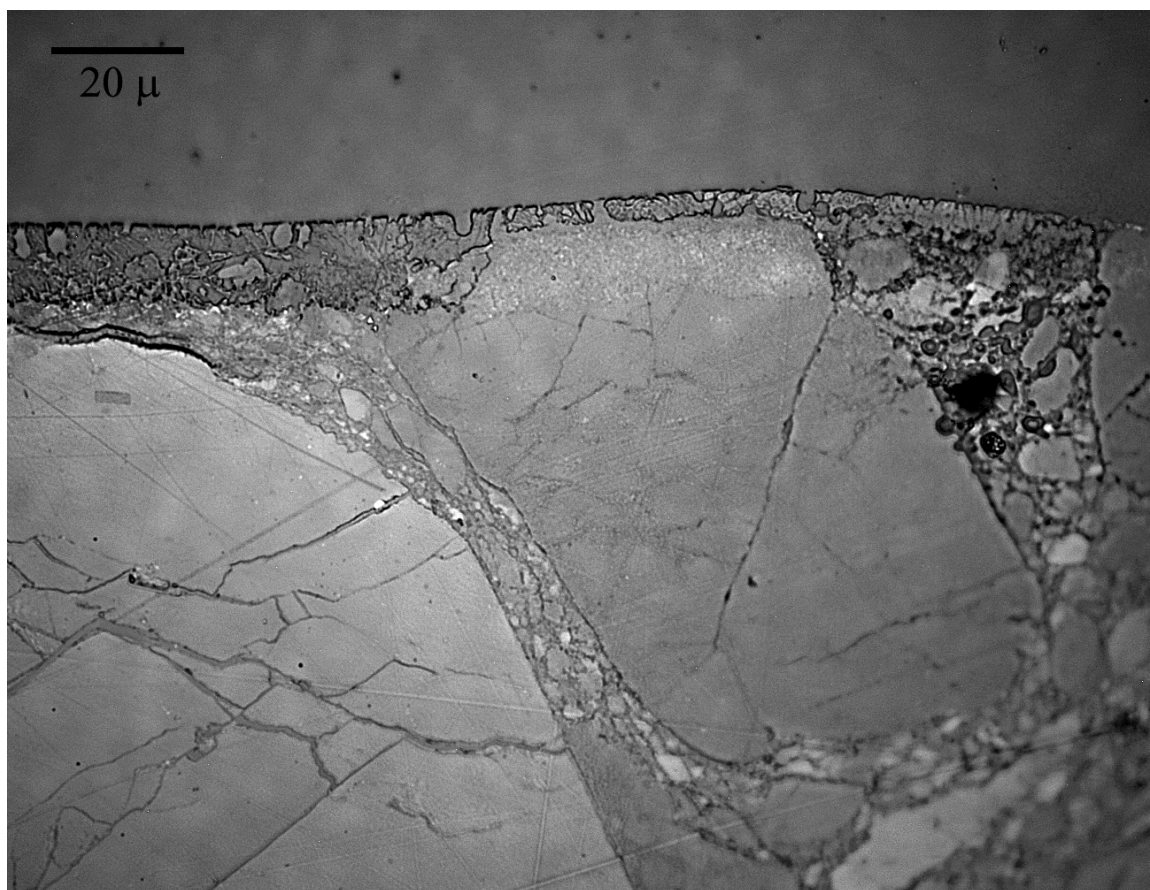


Figure 8. PLM image showing cross-section of melt region in impact zone. Impact was toward top of image.

The surface topology of a typical melt region at two different scales is shown in Figure 9. There is an unmistakable lack of crystalline features as would be typical in a fracture specimen. Rather, the amorphous undulations and holes suggest a frothy melt that was quickly frozen, presumably by a suddenly quenched reaction. This provides a strong corollary to the cross section shown in the PLM image.

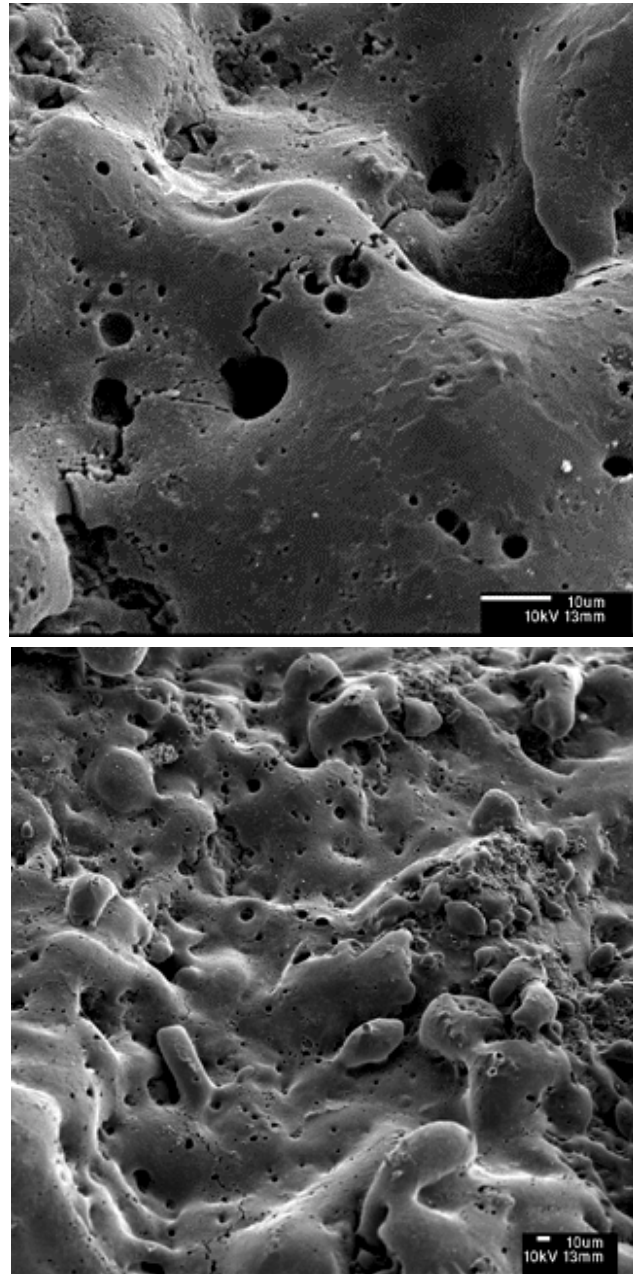


Figure 9. SEM images showing surface topography of melt in impact zone.

PLM and SEM images from this analysis were compared with those from samples of pressed HMX and PBX 9501 that were undisturbed mechanically, but which were burned by flame and quenched suddenly. The conclusion is that for target K8-2174, the mechanical insult from a projectile impact resulted in damage to the PBX 9501 that is typical of solely a thermal insult.

Posttest characterization is ongoing, and other techniques are being investigated to further characterize the damaged state of the PBX 9501. The surfaces of impact-damaged PBX 9501 also showed positive SHG effects, predominantly at the center of the impact location, in the open cracks, and in areas of shear dislocation. These preliminary analyses, coupled with the FTIR reflectance and x-ray powder diffraction (XPD) confirmation data, verify the existence of delta-phase HMX on the top surface of the damaged PBX 9501 up to one year after the initial impact.

MODELING

Calculations using the engineering models DYNA2D and SPRONTO have been performed to support these, and other, low-amplitude insult experiments. These are described in more detail by Scammon et al.¹² The DYNA2D finite element calculations employ an ignition criterion as a function of a characteristic constant, pressure, time, and the maximum shear strain rate to evaluate the threshold level for reaction. The code was originally written with ignition and chemistry models derived from empirical fits to shock-to-detonation-transition (SDT) data, which does not match the mechanical ignition data well. The SPRONTO code is a result of embedding the statistical crack mechanics model, SCRAM, into the mechanical deformation code PRONTO. It solves the one-dimensional heat equation, perpendicular to the planes of penny-shaped cracks, i.e., thin and oblong, excited into two-dimensional grinding motion by the impact, and computes the chemical response of the PBX 9501. These calculations allow us to study pressure and strain rates, to investigate structural aspects of the experiment, and to predict velocities required for reaction. Structural analyses have played an active role in this project beginning with the original target design and continuing through analyses of the experimental results. Alternative designs and various ideas for active instrumentation were examined as part of the experiment evolution process. Predictions of reaction are used to guide these experimental design studies, even though we do not yet have enough experimental data to fully calibrate any of the models.

RESULTS AND DISCUSSION

The violent reaction of the HE resulted in damage and deformation to the retaining ring and cover plate with slight deformation to the inside surface of the holder. No burn or scorch marks were evident on the holder or cover plate in these tests. This is a lower degree of damage than previously witnessed in the large, thick targets described in the report by Idar et al.⁶ This can possibly be attributed to the smaller mass of PBX 9501 available to react. This assumption is further supported by the average energy release, which never exceeded $41 \pm 6\%$ for this target size. Small pieces of PBX 9501 were recovered from each of the reactive events, decreasing in quantity as the projectile velocity was increased. The test numbers, projectile impact velocities, and average energy release data are given in Table 5.

The data for the 10 baseline and 8 aged targets are shown in Figures A-11–A-14 of the appendix. An examination of the strain gauge records provides additional insight regarding the reaction behavior. The back plate strain gauge records show a strong consistency in the impact-induced reaction sequence. See Figure 10 for an example and the appendix for further details on the test performed here. The explosive initially behaves as an elastic-solid, transmitting force to the back plate. Near 2000 microstrain at the back plate, the explosive starts to crush and flow radially. The force levels off and then starts to decrease as the explosive crushes until the annular gap is filled and the pressure on the crushed explosive begins to increase again. A comparison of the data also shows that the delay, ranging from approximately 200 μ s to approximately 400 μ s, between impact to violent reaction decreases as the projectile velocity increases.

Table 5. Test data

Test #	Test Date	PBX 9501 lot ^a	Density (g/cm ³)	Projectile Velocity (m/s)	Test Result	Average Energy Release (%)
K8-2147	09/09/97	730-010	1.830	36.9 \pm 0.8	Quenched	0
K8-2150	09/12/97	730-010	1.830	49.4 \pm 1.1	Quenched	0
K8-2168	10/07/97	730-010	1.831	51.8 \pm 1.2	Quenched	0
K8-2165	09/30/97	730-010	1.831	52.7 \pm 1.2	Quenched	0
K8-2174	10/14/97	730-010	1.830	54.4 \pm 1.3	Quenched	0
K8-2171	10/07/97	730-010	1.830	55.9 \pm 1.3	Violent reaction	16.1 \pm 0.3
K8-2162	09/30/97	730-010	1.831	57.9 \pm 1.3	Violent reaction	32.7 \pm 2.3
K8-2159	09/23/97	730-010	1.830	68.9 \pm 1.6	Violent reaction	34.0 \pm 2.2
K8-2156	09/18/97	730-010	1.831	74.4 \pm 1.7	Violent reaction	35.9 \pm 2.4
K8-2153	09/16/97	730-010	1.830	77.7 \pm 1.8	Violent reaction	37.9 \pm 1.6
K8-2178	10/28/97	730-005	1.840	45.0 \pm 1.0	Quenched	0
K8-2300	11/14/97	685-002	1.840	48.0 \pm 1.1	Quenched	0
K8-2180	10/28/97	730-005	1.841	51.8 \pm 1.2	Quenched	0
K8-2183	11/04/97	730-005	1.840	53.0 \pm 1.2	Violent reaction	17.9 \pm 0.4
K8-2176	10/14/97	730-005	1.840	54.3 \pm 1.2	Violent reaction	41.2 \pm 5.7
K8-2297	11/04/97	685-002	1.840	54.4 \pm 1.3	Violent reaction	21.4 \pm 2.2
K8-2303	11/18/97	685-002	1.840	55.1 \pm 1.3	Violent reaction	36.0 \pm 1.4
K8-2306	11/18/97	685-002	1.841	103.0 \pm 2.4	Violent reaction	39.9 \pm 0.5

^aPBX 9501 lot 730-010 was used in the baseline targets, and lots 685-002 and 730-005 were used in the aged targets.

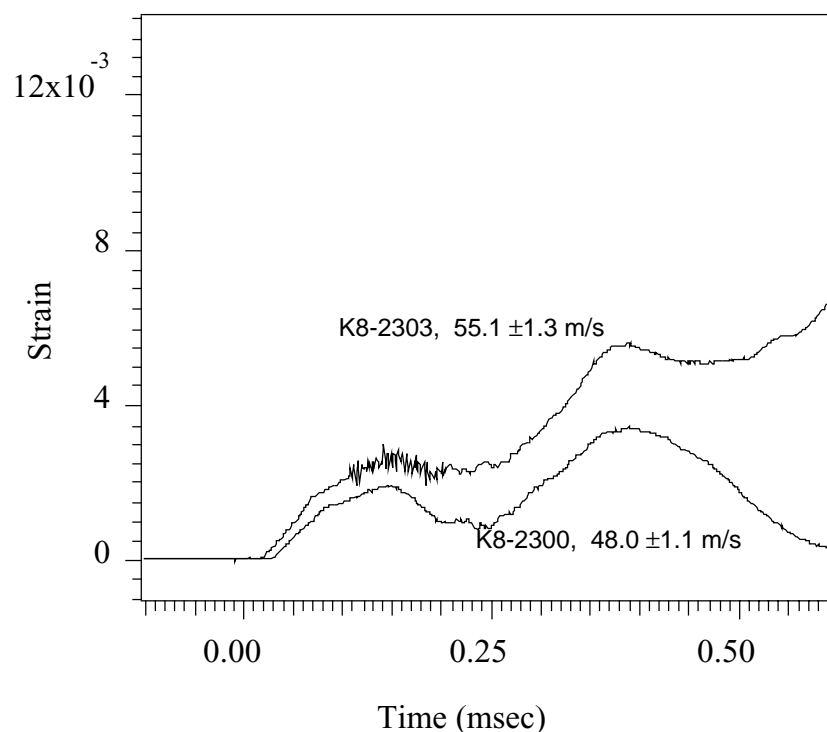


Figure 10. Examples of strain gauge records from tests K8-2300 and K8-2303. Test K8-2303 resulted in a violent reaction, and test K8-2300 was quenched.

Because these strain gauge records clearly show the mechanical behavior and reaction timing of the explosive, they become excellent data for benchmarking the computer codes. As expected, the strain gauge data show the delay to violent reaction relative to impact time decreases as the projectile velocity is increased. At velocities much greater than threshold, the strain records show that the reactive event occurs even before the force on the back plate begins to decrease.

Semiquantitative delays in reaction times can also be determined by comparing the blast gauge time profiles with impact times. The diagnostic data indicates delay times in the blast wave arriving at the gauges decreasing from 2.8 to 1.3 m/s as the projectile velocity is increased to approximately 103 m/s.

A review of the data in both Tables 4 and 5 shows that, with the exception of the K8-2176 test data, as the projectile velocity increases, the dent depth in the holder and the average energy release increase in both baseline and aged targets. In the case of K8-2176 the dent data and average energy release indicate a possible anomaly in the test setup. We postulate that this could be due to a misalignment of the PBX 9501 in the target at the time of projectile impact.

The threshold behavior (see Figure 11) for the small, thin targets demonstrates the same sharp consistency as seen with the large, thick targets of the original test series. The data also do not demonstrate evidence of mixed zone (crossover) results, i.e., violent reactions at lower velocities than the threshold, or nonviolent events at higher velocities that exceed the threshold. Threshold velocities ranged from 54.4 to 55.9 m/s and from 51.8 to 53.0 m/s for the baseline and aged targets, respectively. Based on this threshold shift, it is important to examine possible differences between the baseline and aged PBX 9501 lots.

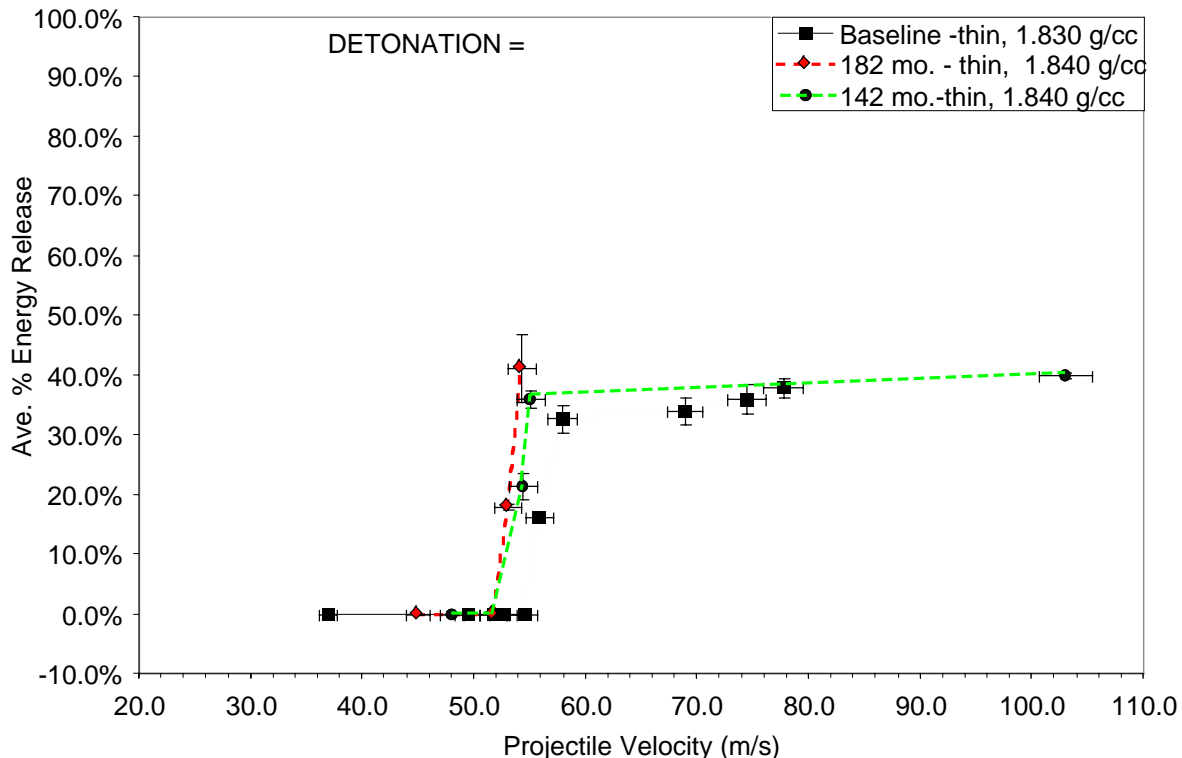


Figure 11. Reaction level for the small, thin Modified Steven targets.

A review of the data in Tables 2 and 3 shows differences in the compositional and GPC analyses of the PBX 9501 library lots, notably weight percent of RDX, weight percent sum of the NP, molecular weight of the Estane 5703, and density. The relative effect of each of these on the threshold response has not been verified. The density difference, 0.01 g/cm^3 , may first appear to be insignificant. The calculated theoretical maximum density (TMD) for PBX 9501 is 1.860 g/cm^3 . The specimens tested here ranged from 98.4 to 98.9% TMD. If the remaining percentage is attributed to porosity, the difference between the two densities is significant. Porosity may play a key role in the time-dependent energy dissipation in the HE after impact.

The effect of density on mechanical ignition events is being explored further with lab-scale, quasi two-dimensional tests.¹³ The initial test results from these experiments show a higher shear strain rate in the 1.830 g/cm^3 PBX 9501 specimen compared with the 1.820 g/cm^3 specimen when impacted under identical conditions. The Modified Steven test threshold

differences between the baseline and aged data are postulated to be due to the differences in densities.

Interestingly, the threshold velocity range for the small, thin targets could be correlated with a pinch of the PBX 9501 between the cover plate and rear surface of the holder. In these tests, the impact of the projectile deforms the cover plate to the extent that it comes in direct contact (pinch) with the inside surface of the holder. This was evident by the circular impact markings on the inside surfaces of the cover plate and holder. Further, a linear regression fit to the projectile velocity as a function of the measured dent of the quenched targets (with the exception of test K8-2174) allows one to extrapolate to a velocity where the PBX 9501 thickness will be fully pinched. This fit corresponded to a velocity of 54.7 ± 0.5 m/s.

SUMMARY

The mechanical loading behavior and response of PBX 9501 have been investigated using Modified Steven target designs. Low-velocity impact was achieved by launching a mild-steel spigot projectile with a powder-driven gun design at PBX 9501 in lightly confined steel targets. The threshold velocities for reaction and violence of reaction for different PBX 9501 lots and histories were evaluated and compared.

Both the baseline and aged target series have demonstrated a remarkably sharp threshold to reaction without evidence of mixed zone results (crossovers). The stockpile-aged samples showed a slight decrease in reaction threshold relative to baseline results. This may be due to the slightly higher densities of the aged materials, variations in the composition, e.g., RDX weight percent, and/or particle size distributions.

Various diagnostics were used to record the timing and target strain behavior relative to projectile impact. The strain gauge records provide evidence for a sequence of events as follows: low-pressure impact, HE material failure, followed by recompaction of the damaged HE, which results in either violent reaction or a quenched event. The gauge data also show that the time scale for the target destruction decreases as a function of increasing projectile velocity.

The physical target evidence and the predictable pinch calculated from the dent profiles of the small, thin targets, suggest that ignition occurs directly under impact. Further work is required to verify this hypothesis.

The violence of reaction, as measured by both passive and active techniques, is reported relative to a detonation in PBX 9501. The recorded violence was never equivalent to a complete detonation of the PBX 9501 and was always delayed relative to a prompt detonation. The highest average energy release recorded was approximately $41 \pm 6\%$. This is lower than the highest average energy release recorded for the large, thick targets of roughly $67 \pm 4\%$.

Posttest characterization of the PBX 9501 quenched and reacted targets is ongoing. Preliminary analysis with PLM and SEM techniques displays evidence of permanent stress-induced twinning in the HMX crystals, melt layer zones, and evidence of gas evolution on the melt layer surface most likely due to reaction. SHG, FTIR, and XPD evidence also

shows that a beta to delta HMX phase transformation has occurred on the surface of the damaged PBX 9501. This provides evidence for a thermal excursion induced by the impact.

Two- and three-dimensional modeling with DYNA2D, SPRONTO, and DYNA3D is concurrent with the experimental work. The calculations have been instrumental in the evolution of the experimental design and testing methods. Front dent deformation data have been used to calibrate the material models for the calculations. Experimental strain and pressure profiles are also being used to benchmark the calculations.

Further work is required (1) to verify the ignition locus(c); (2) to characterize the relative effect of the different projectiles, HE, and confinement variables on the threshold behavior, i.e., an increase or decrease in threshold; and (3) to determine a semiquantitative relationship for the threshold behavior as a function of the different variables.

ACKNOWLEDGEMENTS

We gratefully acknowledge the support of the following groups and individuals in these research activities: Phil Howe, George Hurley, and Luis Salazar for programmatic and technical support; Dick Scammon, Richard Browning, John Dienes, and John Middleditch for analytical modeling support; Phil Berry and coworkers of ESA-MT, and Greg Cunningham and Jim Harsh of DX-3 for x-rays and radiographic numerical analyses. We also thank Steve Chidester of Lawrence Livermore National Laboratory for his helpful suggestions regarding this research. The experimental results reported here have been a successful culmination of numerous individual efforts. Accordingly, we would also like to acknowledge the following contributions to this project: JCI-NTS shop, the DX-5 technicians, the DX-5 designers and machinists, the DX-4 firing site support staff, the ESA-WMM assembly crew, and Aaron Honey, DX-3, for his image work and documentation.

REFERENCES

1. L. G. Green and G. D. Dorough, "Further Studies on the Ignition of Explosives," Fourth International Detonation Symposium, ARC-126, Office of Naval Research - Department of the Navy, Washington, D.C., pp. 477–486, 1965.
2. S. K. Chidester, L. G. Green, and C. G. Lee, "A Frictional Work Predictive Method for the Initiation of Solid High Explosives from Low-Pressure Impacts," Tenth International Detonation Symposium, Office of Naval Research, Arlington, Virginia, pp. 786–792, 1993.
3. S. K. Chidester, C. M. Tarver, and C. G. Lee, "Impact Ignition of New and Aged Solid Explosives," 1997 American Physical Society Topical Conference on Shock Compression of Condensed Matter, AIP Conference Proceedings 429, Woodbury, New York, pp. 707–710, 1997.
4. S. K. Chidester and C. M. Tarver, "Safety of Stockpile Aged Energetic Materials," 1998 Life Cycles of Energetic Materials Conference, Fullerton, CA, Mar. 29–Apr. 1, 1998.

5. S. K. Chidester and C. M. Tarver, "Low-Amplitude Impact Testing and Analysis of Pristine and Aged High Explosives," Eleventh International Detonation Symposium, Snowmass, CO, Aug. 31–Sept. 4, 1998.
6. D. J. Idar, R. A. Lucht, R. J. Scammon, J. W. Straight, and C. B. Skidmore, "PBX 9501 High Explosive Violent Response/Low Amplitude Insult Project: Phase I," Los Alamos National Laboratory report LA-13164-MS, Los Alamos, NM (January 1997).
7. D. J. Idar, R. A. Lucht, J. W. Straight, R. J. Scammon, R. V. Browning, J. Middleditch, J. K. Dienes, C. B. Skidmore, and G. A. Buntain, "Low Amplitude Insult Project: PBX 9501 High Explosive Violent Reaction Experiments," Eleventh International Detonation Symposium, Snowmass, CO, Aug. 31–Sept. 4, 1998.
8. "Adhesives Technology of Estane Polyurethane," B. F. Goodrich Specialty Chemicals, TSR 76-02 TF116, March 1995.
9. D. S. Phillips, C. B. Skidmore, D. J. Idar, S. F. Son, R. B. Schwarz, and B. W. Asay, "Defect Structures in Some Insulted HMX Composites," Inter/Micro 98, Chicago, IL, Aug. 10–14, 1998.
10. C. B. Skidmore, D. S. Phillips, D. J. Idar, and S. F. Son, "Characterizing the Microstructure of Selected High Explosives," Europyro '99, Brest, France, June 7–11, 1999.
11. B. F. Henson, R. K. Sander, S. F. Son, J. M. Robinson, P. M. Dickson, and B. W. Asay, "Measurement of the HMX β -to- δ Phase Transition by Second Harmonic Generation," *Phys. Rev. Lett.* **82**(6) pp. 213–216. (May 1998).
12. R. J. Scammon, R. V. Browning, J. Middleditch, J. K. Dienes, K. S. Haberman, and J. G. Bennett, "Low Amplitude Insult Project: Structural Analysis and Prediction of Low Order Reaction," Eleventh International Detonation Symposium, Snowmass, CO, Aug. 31–Sept. 4, 1998.
13. B. W. Asay, P. M. Dickson, B. Henson, C. S. Fugard, D. J. Funk, and D. J. Idar, "Dynamic Measurement of the Influence of Projectile Radius and Velocity on Strain Localization During Impact of an Energetic Material," Eleventh International Detonation Symposium, Snowmass, CO, Aug. 31–Sept. 4, 1998.

APPENDIX

Target dent, strain gauge, and radiographic data

The front dent data were obtained by identifying the top-to-bottom and left-to-right axes and by taking measurements through the impact point and center. These depth data are given as a function of distance across the surface of the target cover plate or inside surface of the holder. Typically, if impact did not occur on center, the front dent data was measured twice, once through the impact (IMPACT) point, and once through the center (CENTER) face of the target. Any exceptions are noted otherwise in the body of the text. The first two tables are copies of tables in the main body of the report, and are meant to provide a quick correlation to the dent and deformation data.

The dent data are given in the appendix in order of baseline data followed by aged data of increasing velocity. These data are followed by the numerically digitized and enhanced images of the radiographs of the damaged targets. High-energy x-rays, 2.2 MeV, were used to obtain posttest radiographs of the damaged and quenched targets. Targets were radiated for approximately 1 minute at 2.2 MeV using a film/screen stack consisting of the following 5 layers: (1) 0.010-in. thick lead, (2) M film, (3) 0.003-in. thick lead, (4) M film, and (5) 0.010-in. thick lead.

The radiographs were digitized and enhanced with numerical methods to further evaluate the crack variations in the HE after impact. The dark center on the enhanced image is produced as an artifact of the numerical enhancement method.

Table A-1. Target test dates, PBX 9501 lots, densities, projectile velocities, test results, and average energy release

Test #	Test Date	PBX 9501 lot ^a	Density (g/cm ³)	Projectile Velocity (m/s)	Test Result	Average Energy Release %
K8-2147	09/09/97	730-010	1.830	36.9 ±0.8	Quenched	0
K8-2150	09/12/97	730-010	1.830	49.4 ±1.1	Quenched	0
K8-2168	10/07/97	730-010	1.831	51.8 ±1.2	Quenched	0
K8-2165	09/30/97	730-010	1.831	52.7 ±1.2	Quenched	0
K8-2174	10/14/97	730-010	1.830	54.4 ±1.3	Quenched	0
K8-2171	10/07/97	730-010	1.830	55.9 ±1.3	Violent reaction	16.1 ±0.3
K8-2162	09/30/97	730-010	1.831	57.9 ±1.3	Violent reaction	32.7 ±2.3
K8-2159	09/23/97	730-010	1.830	68.9 ±1.6	Violent reaction	34.0 ±2.2
K8-2156	09/18/97	730-010	1.831	74.4 ±1.7	Violent reaction	35.9 ±2.4
K8-2153	09/16/97	730-010	1.830	77.7 ±1.8	Violent reaction	37.9 ±1.6
K8-2178	10/28/97	730-005	1.840	45.0 ±1.0	Quenched	0
K8-2300	11/14/97	685-002	1.840	48.0 ±1.1	Quenched	0
K8-2180	10/28/97	730-005	1.841	51.8 ±1.2	Quenched	0
K8-2183	11/04/97	730-005	1.840	53.0 ±1.2	Violent reaction	17.9 ±0.4
K8-2176	10/14/97	730-005	1.840	54.3 ±1.2	Violent reaction	41.2 ±5.7
K8-2297	11/04/97	685-002	1.840	54.4 ±1.3	Violent reaction	21.4 ±2.2
K8-2303	11/18/97	685-002	1.840	55.1 ±1.3	Violent reaction	36.0 ±1.4
K8-2306	11/18/97	685-002	1.841	103.0 ±2.4	Violent reaction	39.9 ±0.5

^aPBX 9501 lot 730-010 was used in the baseline targets, and lots 685-002 and 730-005 were used in the aged targets.

Table A-2. Target projectile velocities, impact point, and average measured dent depths

Test #	Projectile Velocity (m/s)	Impact Point	Average Measured Dent Depth on Cover Plate (mm)	Average Measured Dent Depth on Inside Surface of Holder (mm)
K8-2147	36.9 ±0.8	On center left-to-right, 0.1875-in. high	8.26 ±0.02	
K8-2150	49.4 ±1.1	0.375-in. left, 0.125-in. high	11.26 ±0.03	
K8-2168	51.8 ±1.2	0.125-in. right, 0.1875-in. high	11.89 ±0.19	
K8-2165	52.7 ±1.2	0.375-in. right, 0.50-in. high	12.37 ±0.08	
K8-2174	54.4 ±1.3	0.5-in. left, 0.5-in. low	10.99 ±0.37 ^a	
K8-2171	55.9 ±1.3	0.1875-in. left, 0.1875-in. high		0.25 ±0.10
K8-2162	57.9 ±1.3	0.50-in. right, 0.50-in. high		0.24 ±0.01
K8-2159	68.9 ±1.6	0.25-in. left, on center high to low		0.75 ±0.02
K8-2156	74.4 ±1.7	0.5-in. right, 0.1875-in. high		1.88 ±0.09
K8-2153	77.7 ±1.8	0.25-in. right, 0.375-in. high		2.46 ±0.26
K8-2178	45.0 ±1.0	0.375-in. left, 0.25-in. low	10.32 ±0.16	
K8-2300	48.0 ±1.1	0.4375-in. right, 0.5-in. high	10.44 ±0.03	
K8-2180	51.8 ±1.2	0.125-in. right, on center high to low	11.88 ±0.01	
K8-2183	53.0 ±1.2	0.5-in. left, 0.125-in. high		0.15 ±0.01
K8-2176	54.3 ±1.2	0.125-in. right, and 0.125-in. high		1.51 ±0.08
K8-2297	54.4 ±1.3	0.125-in. right, 0.125-in. high		0.27 ±0.17
K8-2303	55.1 ±1.3	On center		0.30 ±0.01
K8-2306	103.0 ±2.4	On center left-to-right, 0.25-in. high		6.09 ±0.11

^aThe dent measurement on the stainless steel cover plate of test K8-2174 was obtained after the cover was removed from the target.

Target data for baseline PBX 9501 material

Table A-3. Quenched target K8-2147 dent data. Impact occurred on center left-to-right, and 0.1875-in. high of center at 36.9 ± 0.8 m/s. The average measured dent depth was 8.26 ± 0.02 mm.

Distance (inches)	Center Left-to-right (inches)	Center Top-to-bottom (inches)	Impact Left-to-right (inches)	Impact Top-to-bottom (inches)
0.00	0.0000	0.0000	0.0000	0.0000
0.20	0.0016	0.0026	0.0013	0.0019
0.39	0.0004	0.0036	0.0013	0.0042
0.59	-0.0039	0.0021	-0.0060	0.0044
0.79	-0.0245	-0.0020	-0.0242	0.0023
0.98	-0.0630	-0.0159	-0.0639	-0.0136
1.18	-0.1093	-0.0351	-0.1339	-0.0400
1.38	-0.1977	-0.1037	-0.2275	-0.0962
1.57	-0.2618	-0.1827	-0.2798	-0.1726
1.77	-0.2979	-0.2618	-0.3102	-0.2601
1.97	-0.2935	-0.2950	-0.3260	-0.2993
2.17	-0.2665	-0.3109	-0.3194	-0.3247
2.36	-0.2106	-0.3155	-0.3008	-0.3226
2.56	-0.1375	-0.2913	-0.2668	-0.2813
2.76	-0.0614	-0.2311	-0.2020	-0.2027
2.95	-0.0305	-0.1529	-0.1256	-0.1486
3.15	-0.0049	-0.0737	-0.0652	-0.0241
3.35	0.0027	-0.0332	-0.0304	-0.0229
3.54	0.0046	-0.0104	-0.0041	-0.0070
3.74	0.0041	-0.0018	0.0021	-0.0009
3.94	0.0016	0.0000	0.0014	0.0000
4.13	-0.0017	-0.0019	0.0000	-

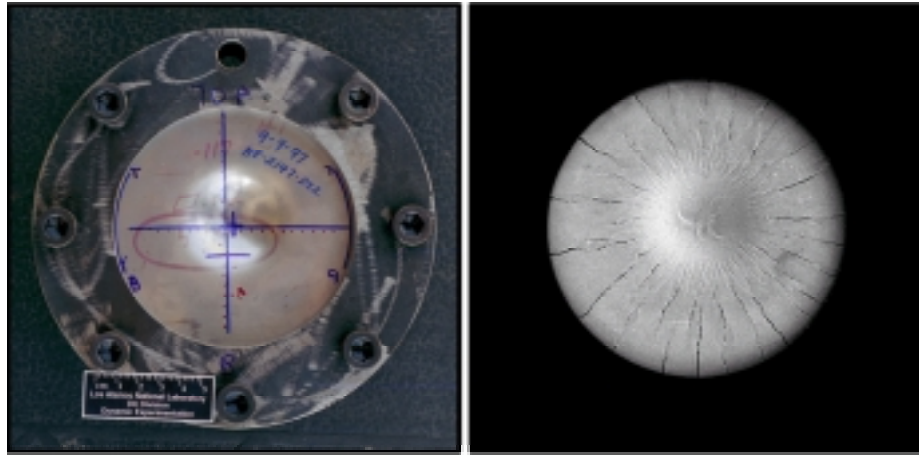


Figure A-1. Target K8-2147 35-mm images with and without cover plate. The PBX 9501 shows evidence of radial cracking on the surface.

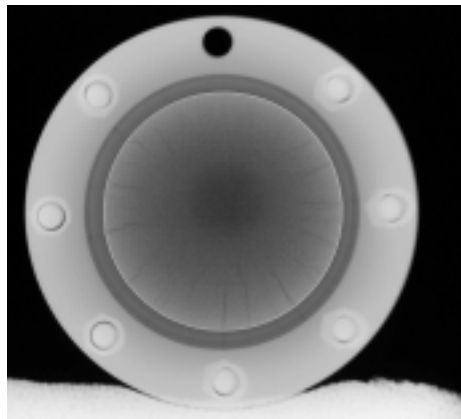


Figure A-2. Radiograph of target K8-2147.

Table A-4. Quenched Target K8-2150 dent data. Impact occurred 0.375-in. to the left and 0.125-in. high of center at 49.4 ± 1.1 m/s. The average measured dent depth was 11.26 ± 0.13 mm.

Distance (inches)	Center Left-to-right (inches)	Center Top-to-bottom (inches)	Impact Left-to-right (inches)	Impact Top-to-bottom (inches)
0.00	0.0000	0.0000	0.0000	0.0000
0.20	0.0083	0.0079	0.0080	0.0109
0.39	0.0082	0.0111	0.0075	0.0105
0.59	-0.0044	-0.0210	0.0039	-0.0096
0.79	-0.0386	-0.0321	-0.0509	-0.0437
0.98	-0.1033	-0.1022	-0.1107	-0.1073
1.18	-0.2006	-0.2063	-0.2094	-0.2069
1.38	-0.3077	-0.3214	-0.3195	-0.3163
1.57	-0.3846	-0.3991	-0.3775	-0.3791
1.77	-0.4308	-0.4330	-0.4261	-0.4009
1.97	-0.4398	-0.4313	-0.4469	-0.4395
2.17	-0.4203	-0.4046	-0.4370	-0.4278
2.36	-0.3633	-0.3412	-0.4031	-0.3767
2.56	-0.3077	-0.2480	-0.3434	-0.2826
2.76	-0.2284	-0.1410	-0.2208	-0.1716
2.95	-0.0996	-0.0679	-0.1139	-0.1007
3.15	-0.0527	-0.0210	-0.0390	-0.0323
3.35	0.0006	0.0059	-0.0001	0.0013
3.54	0.0148	0.0153	-0.0166	0.0186
3.74	0.0144	0.0142	-0.0240	0.0219
3.94	0.0127	0.0068	-0.0207	0.0168
4.13	0.0040	-0.0030	-0.0111	0.0063

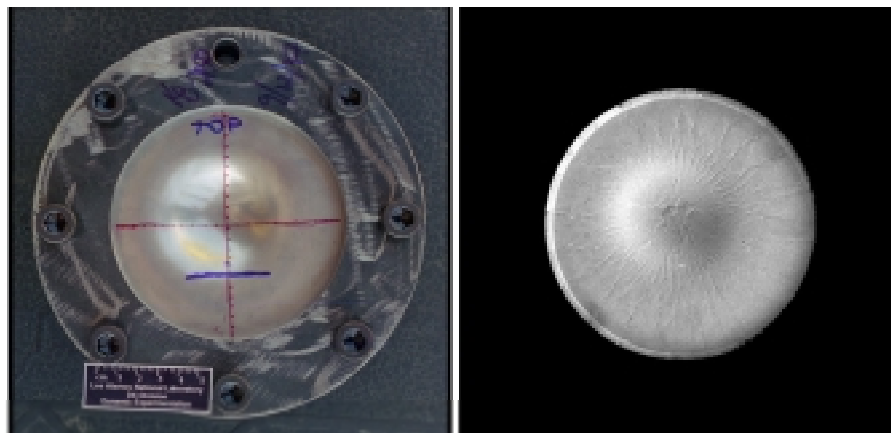


Figure A-3. Target K8-2150 35-mm images with and without cover plate. The PBX 9501 shows evidence of radial cracks, with little space between them.

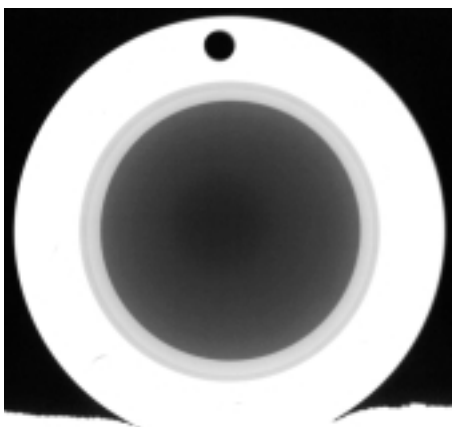


Figure A-4. Radiograph of target K8-2150. Radiograph does not display any evidence of cracks through the HE thickness.

Table A-5. Quenched target K8-2168 dent data. Impact occurred 0.125-in. to the right, and 0.1875-in. high of center at 51.8 ± 1.2 m/s. The average measured dent depth on the cover plate was 11.89 ± 0.19 mm.

Distance (inches)	Center Left-to-right (inches)	Center Top-to-bottom (inches)	Impact Left-to-right (inches)	Impact Top-to-bottom (inches)
0.00	0.0000	0.0000	0.0000	0.0000
0.20	-0.0080	0.0048	-0.0059	0.0002
0.39	-0.0460	0.0017	-0.0427	0.0018
0.59	-0.1095	-0.0155	-0.1386	-0.0040
0.79	-0.2205	-0.0681	-0.2645	-0.0229
0.98	-0.3125	-0.1398	-0.3593	-0.0727
1.18	-0.3860	-0.2934	-0.4302	-0.1476
1.38	-0.4455	-0.3846	-0.4626	-0.2664
1.57	-0.4615	-0.4303	-0.4604	-0.3682
1.77	-0.4450	-0.4439	-0.4538	-0.4551
1.97	-0.3960	-0.4256	-0.4072	-0.4734
2.17	-0.3360	-0.3587	-0.3451	-0.4573
2.36	-0.2475	-0.2909	-0.2454	-0.4036
2.56	-0.1300	-0.1841	-0.1403	-0.3159
2.76	-0.0585	-0.0842	-0.0697	-0.1848
2.95	-0.0175	-0.0394	-0.0320	-0.1141
3.15	0.0010	-0.0130	-0.0009	-0.0510
3.35	0.0095	-0.0002	0.0027	-0.0143
3.54	0.0050	0.0022	0.0034	0.0078
3.74	0.0000	0.0000	0.0000	0.0000

Table A-6. Quenched target K8-2165 dent data. Impact occurred 0.375-in. to the right, and 0.5-in. high of center at 52.7 ± 1.2 m/s. The average measured dent depth on the cover plate was 12.37 ± 0.08 mm.

Distance (inches)	Center Left-to-right (inches)	Center Top-to-bottom (inches)	Impact Left-to-right (inches)	Impact Top-to-bottom (inches)
0.00	0.0000	0.0000	0.0000	0.0000
0.20	0.0028	0.0137	-0.0062	0.0057
0.39	0.0025	0.0282	-0.0295	0.0158
0.59	-0.0144	0.0413	-0.0932	0.0195
0.79	-0.0453	0.0454	-0.2089	0.0136
0.98	-0.0945	0.0432	-0.3812	-0.0117
1.18	-0.1679	0.0293	-0.4559	-0.0521
1.38	-0.2288	-0.0032	-0.4891	-0.1139
1.57	-0.3175	-0.0591	-0.4809	-0.2162
1.77	-0.3396	-0.1278	-0.4371	-0.3331
1.97	-0.3350	-0.2403	-0.3714	-0.4024
2.17	-0.2971	-0.3049	-0.2776	-0.4663
2.36	-0.2280	-0.4155	-0.1748	-0.4846
2.56	-0.1379	-0.4493	-0.1001	-0.4574
2.76	-0.0742	-0.4523	-0.0508	-0.4158
2.95	-0.0211	-0.4197	-0.0195	-0.3456
3.15	0.0074	-0.3680	-0.0038	-0.2520
3.35	0.0123	-0.2799	0.0000	-0.1203
3.54	0.0222	-0.1678	-	-0.0492
3.74	0.0197	-0.0894	-	0.0000
3.94	0.0141	-0.0413	-	-
4.13	0.0065	-0.0135	-	-

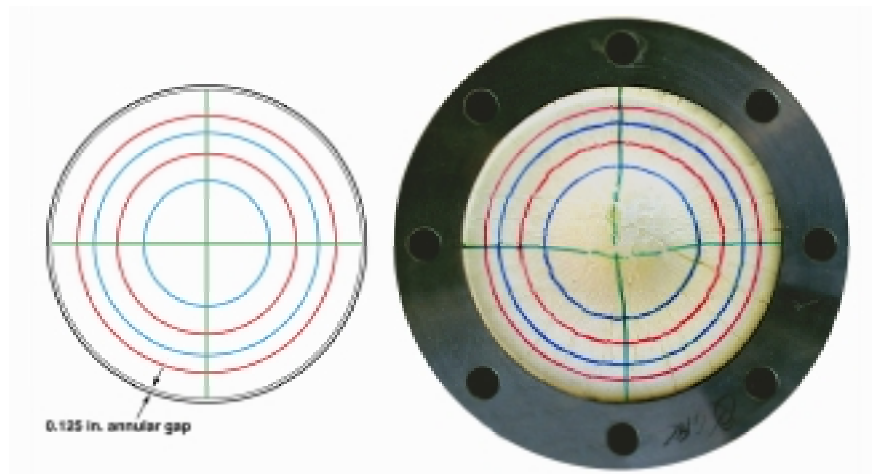


Figure A-5. Target K8-2174 35 mm image. The left-hand drawing shows the concentric circles as drawn on the PBX 9501 before impact. The surface of the PBX 9501 in this target shows evidence of material dislocation and radial crack formation.

Table A-7. Quenched target K8-2174 dent data. Impact occurred 0.5-in. left, and 0.5-in. low of center at 54.4 ± 1.3 m/s. The average dent depth on the cover plate was 10.99 ± 0.37 mm. NOTE: Cover was removed before dent data was measured.

Distance (inches)	Center Left-to-right (inches)	Center Top-to-bottom (inches)	Impact Left-to-right (inches)	Impact Top-to-bottom (inches)
0.00	0.0000	0.0000	0.0000	0.0000
0.20	0.0485	0.0204	0.0342	-0.0042
0.39	0.0675	0.0328	0.0714	-0.0194
0.59	0.0995	0.0292	0.1326	-0.0916
0.79	0.1070	0.0271	0.1214	-0.2048
0.98	0.1040	-0.0825	0.1346	-0.2910
1.18	0.0790	-0.1870	0.1043	-0.3717
1.38	0.0255	-0.2411	0.0410	-0.4164
1.57	-0.0165	-0.2947	-0.0778	-0.4226
1.77	-0.1195	-0.2363	-0.1876	-0.3983
1.97	-0.2210	-0.1199	-0.2669	-0.3870
2.17	-0.2805	-0.0670	-0.2956	-0.2787
2.36	-0.3200	-0.0076	-0.3034	-0.1719
2.56	-0.3010	0.0328	-0.3042	-0.0676
2.76	-0.2575	0.0317	-0.2335	-0.0163
2.95	-0.1910	0.0311	-0.1928	0.0000
3.15	-0.1605	0.0175	-0.0491	-0.0067
3.35	-0.0330	-0.0080	0.0741	-0.0099
3.54	0.0390	—	0.1029	-0.0116
3.74	0.0765	—	0.1346	-0.0293
3.94	0.1070	—	0.1388	—

Table A-8. Target K8-2171, inside surface, dent data. Data was only obtained for the impact point. The center point did not have any measurable deformation. Impact occurred 0.1875-in. left, and 0.1875-in. high of center at 55.9 ± 1.3 m/s. The average measured dent depth on the inside surface of the holder was 0.25 ± 0.10 mm.

Distance (inches)	Impact Left-to-right (inches)	Impact Top-to-bottom (inches)
0.00	0.0000	0.0000
0.20	-0.0011	0.0000
0.39	-0.0011	-0.0010
0.59	-0.0022	-0.0040
0.79	-0.0023	-0.0050
0.98	-0.0033	-0.0040
1.18	-0.0044	-0.0050
1.38	-0.0044	-0.0070
1.57	-0.0055	-0.0060
1.77	-0.0056	-0.0070
1.97	-0.0056	-0.0070
2.17	-0.0127	-0.0070
2.36	-0.0058	-0.0070
2.56	-0.0058	-0.0070
2.76	-0.0054	-0.0060
2.95	-0.0044	-0.0060
3.15	-0.0040	-0.0050
3.35	-0.0036	-0.0050
3.54	-0.0031	-0.0050
3.74	-0.0027	-0.0045
3.94	-0.0023	-0.0030
4.13	-0.0018	-0.0025
4.33	-0.0009	-0.0010
4.53	-0.0004	-0.0005
4.72	0.0000	0.0000



Figure A-6. PBX 9501 fragments retrieved from the firing mound from test K8-2171. Each of the violent reaction tests resulted in HE dispersal on the firing mound.

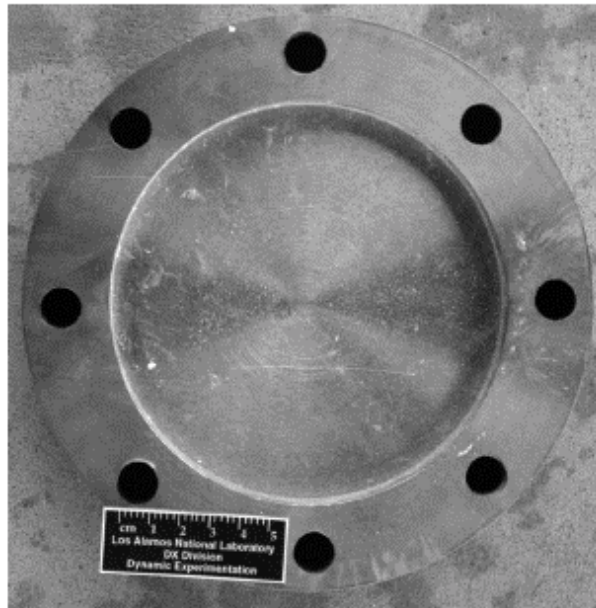
Table A-9. Target K8-2162, inside surface, dent data. Impact occurred 0.50-in. to the right, and 0.50-in. high of center. The average measured dent depth on the inside surface of the holder was 0.24 ± 0.01 mm.

Distance (inches)	Center Left-to-right (inches)	Center Top-to-bottom (inches)	Impact Left-to-right (inches)	Impact Top-to-bottom (inches)
0.00	0.0000	0.0000	0.0000	0.0000
0.20	-0.0014	-0.0011	0.0000	0.0000
0.39	-0.0028	-0.0017	-0.0009	-0.0019
0.59	-0.0093	-0.0026	-0.0016	-0.0027
0.79	-0.0104	-0.0036	-0.0029	-0.0037
0.98	-0.0121	-0.0049	-0.0042	-0.0048
1.18	-0.0129	-0.0060	-0.0054	-0.0050
1.38	-0.0144	-0.0069	-0.0070	-0.0068
1.57	-0.0158	-0.0082	-0.0081	-0.0075
1.77	-0.0157	-0.0085	-0.0089	-0.0086
1.97	-0.0148	-0.0088	-0.0096	-0.0089
2.17	-0.0151	-0.0092	-0.0093	-0.0089
2.36	-0.0158	-0.0094	-0.0092	-0.0090
2.56	-0.0149	-0.0091	-0.0089	-0.0082
2.76	-0.0134	-0.0081	-0.0082	-0.0077
2.95	-0.0125	-0.0077	-0.0073	-0.0066
3.15	-0.0116	-0.0064	-0.0066	-0.0051
3.35	-0.0103	-0.0048	-0.0050	-0.0038
3.54	-0.0094	-0.0030	-0.0037	-0.0027
3.74	-0.0082	-0.0020	-0.0026	-0.0016
3.94	-0.0076	-0.0010	-0.0014	-0.0005
4.13	-0.0064	—	0.0002	0.0004

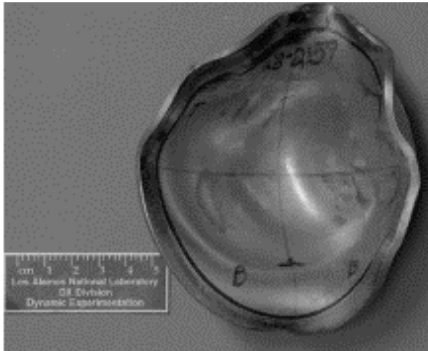
Table A-10. Target K8-2159, inside surface, data. Impact occurred 0.25-in. to the left of center, and on center top-to-bottom at 68.9 ± 1.6 m/s. The average measured dent depth on the inside surface of the holder was 0.75 ± 0.02 mm.

Distance (inches)	Center Left-to-right (inches)	Center Top-to-bottom (inches)	Impact Left-to-right (inches)	Impact Top-to-bottom (inches)
0.00	0.0000	0.0000	0.0000	0.0000
0.20	-0.0028	-0.0028	-0.0029	-0.0024
0.39	-0.0052	-0.0058	-0.0056	-0.0054
0.59	-0.0082	-0.0094	-0.0088	-0.0092
0.79	-0.0112	-0.0136	-0.0121	-0.0125
0.98	-0.0142	-0.0170	-0.0158	-0.0161
1.18	-0.0180	-0.0203	-0.0185	-0.0199
1.38	-0.0212	-0.0227	-0.0222	-0.0232
1.57	-0.0238	-0.0252	-0.0248	-0.0254
1.77	-0.0252	-0.0302	-0.0263	-0.0274
1.97	-0.0252	-0.0299	-0.0288	-0.0300
2.17	-0.0249	-0.0246	-0.0269	-0.0279
2.36	-0.0228	-0.0235	-0.0241	-0.0283
2.56	-0.0204	-0.0195	-0.0211	-0.0273
2.76	-0.0175	-0.0170	-0.0176	-0.0254
2.95	-0.0141	-0.0139	-0.0141	-0.0222
3.15	-0.0110	-0.0105	-0.0101	-0.0199
3.35	-0.0082	-0.0069	-0.0072	-0.0169
3.54	-0.0052	-0.0050	-0.0044	-0.0142
3.74	-0.0022	-0.0024	-0.0006	-0.0110
3.94	0.0008	-0.0011	—	-0.0090
4.13	0.0038	0.0015	—	—

(a) K8-2159 steel holder



(b) K8-2159 front surface of cover plate



(c) K8-2159 back surface of cover plate

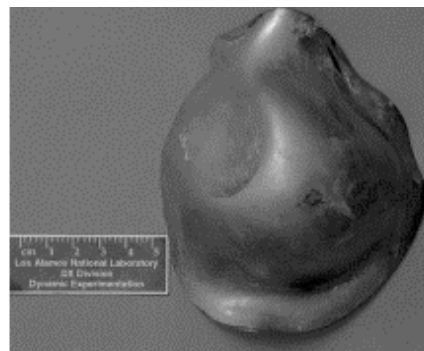
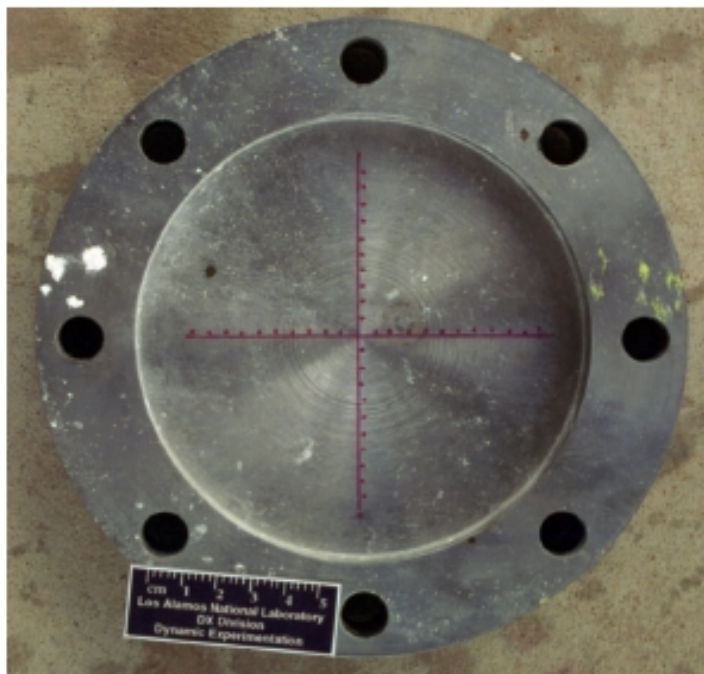


Figure A-7(a-c). Target K8-2159 posttest images of the steel holder and stainless steel cover plate. The holder does not show any significant evidence of damage, other than a small indentation from the impact. The cover plate is deformed, but intact.

Table A-11. Target K8-2156, inside surface, dent data. Target was impacted 0.50-in. to the right of center, and 0.1875-in. high at 74.4 ± 1.7 m/s. The average measured dent depth on the inside surface of the holder was 1.88 ± 0.09 mm.

Distance (inches)	Center Left-to-right (inches)	Center Top-to-bottom (inches)	Impact Left-to-right (inches)	Impact Top-to-bottom (inches)
0.00	0.0000	0.0000	0.0000	0.0000
0.20	-0.0073	-0.0078	-0.0052	-0.0061
0.39	-0.0154	-0.0162	-0.0126	-0.0136
0.59	-0.0216	-0.0237	-0.0211	-0.0217
0.79	-0.0344	-0.0330	-0.0292	-0.0291
0.98	-0.0418	-0.0409	-0.0381	-0.0392
1.18	-0.0495	-0.0503	-0.0452	-0.0457
1.38	-0.0572	-0.0583	-0.0558	-0.0541
1.57	-0.0621	-0.0634	-0.0618	-0.0605
1.77	-0.0671	-0.0699	-0.0708	-0.0646
1.97	-0.0687	-0.0731	-0.0764	-0.0673
2.17	-0.0674	-0.0744	-0.0739	-0.0675
2.36	-0.0636	-0.0741	-0.0694	-0.0712
2.56	-0.0576	-0.0731	-0.0652	-0.0674
2.76	-0.0529	-0.0623	-0.0578	-0.0574
2.95	-0.0435	-0.0552	-0.0501	-0.0468
3.15	-0.0345	-0.0459	-0.0415	-0.0397
3.35	-0.0265	-0.0380	-0.0327	-0.0284
3.54	-0.0178	-0.0280	-0.0240	-0.0177
3.74	-0.0101	-0.0187	-0.0167	-0.0090
3.94	-0.0031	-0.0096	-0.0100	-0.0012
4.13	0.0053	-0.0031	—	—

(a) K8-2156 steel holder



(b) K8-2156 PBX 9501, posttest

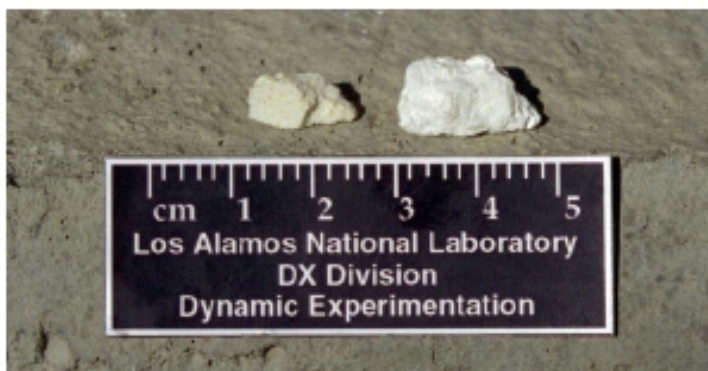


Figure A-8(a-b). Target K8-2156 posttest images of the holder and PBX 9501 retrieved from the firing mound.

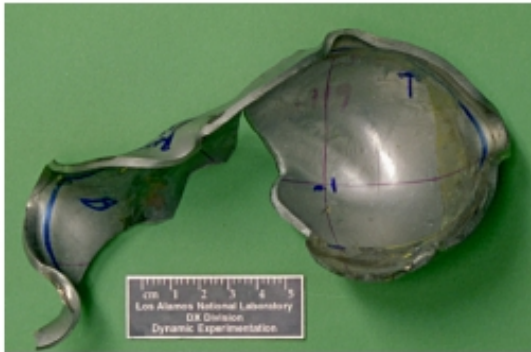
Table A-12. Target K8-2153, inside surface, dent data. Target was impacted 0.25-in. to the right, and 0.375-in. high of center at 77.7 ± 1.8 m/s. The average measured dent depth on the inside surface of the holder was 2.46 ± 0.26 mm.

Distance (inches)	Center Left-to-right (inches)	Center Top-to-bottom (inches)	Impact Left-to-right (inches)	Impact Top-to-bottom (inches)
0.00	0.0000	0.0000	0.0000	0.0000
0.20	-0.0160	-0.0120	-0.0113	-0.0142
0.39	-0.0292	-0.0252	-0.0209	-0.0292
0.59	-0.0415	-0.0397	-0.0343	-0.0451
0.79	-0.0555	-0.0539	-0.0495	-0.0568
0.98	-0.0686	-0.0650	-0.0636	-0.0690
1.18	-0.0820	-0.0781	-0.0760	-0.0787
1.38	-0.0925	-0.0894	-0.0875	-0.0849
1.57	-0.1027	-0.0990	-0.0981	-0.0899
1.77	-0.1067	-0.1050	-0.1041	-0.0871
1.97	-0.1049	-0.1078	-0.1036	-0.0753
2.17	-0.1006	-0.1078	-0.1005	-0.0666
2.36	-0.0932	-0.1068	-0.0945	-0.0534
2.56	-0.0841	-0.1015	-0.0856	-0.0425
2.76	-0.0727	-0.0939	-0.0758	-0.0282
2.95	-0.0628	-0.0824	-0.0683	-0.0167
3.15	-0.0505	-0.0696	-0.0519	-0.0014
3.35	-0.0327	-0.0536	-0.0392	0.0100
3.54	-0.0216	-0.0417	-0.0267	0.0220
3.74	-0.0069	-0.0280	-0.0140	—
3.94	0.0053	-0.0165	-0.0038	—
4.13	0.0147	-0.0044	—	—

(a) K8-2156 steel holder



(b) K8-2153, front surface of cover plate



(c) K8-2153, back surface of cover plate



Figure A-9(a-c). Target K8-2153 posttest images of the holder and cover plate. The holder does not show any significant evidence of damage other than a small indentation from the impact. The cover plate is deformed and sheared.

Target data for aged PBX 9501 material

Table A-13. Quenched target K8-2178 dent data. Impact occurred 0.375-in. to the left, and 0.25-in. low of center at 45.0 ± 1.0 m/s. The average measured dent depth on the cover plate was 10.32 ± 0.16 mm.

Distance (inches)	Center Left-to-right (inches)	Center Top-to-bottom (inches)	Impact Left-to-right (inches)	Impact Top-to-bottom (inches)
0.00	0.0000	0.0000	0.0000	0.0000
0.20	0.0046	0.0015	0.0051	0.0014
0.39	0.0083	-0.0014	0.0091	-0.0052
0.59	0.0074	-0.0264	0.0092	-0.0533
0.79	-0.0019	-0.0794	-0.0013	-0.1179
0.98	-0.0268	-0.1589	-0.0287	-0.2040
1.18	-0.0711	-0.2713	-0.0727	-0.3086
1.38	-0.1335	-0.3393	-0.1511	-0.3762
1.57	-0.2328	-0.3863	-0.2401	-0.4018
1.77	-0.3262	-0.3883	-0.3280	-0.4109
1.97	-0.3720	-0.3567	-0.3745	-0.3936
2.17	-0.3974	-0.3197	-0.4019	-0.3402
2.36	-0.4007	-0.2332	-0.3939	-0.2633
2.56	-0.3686	-0.1342	-0.3468	-0.1649
2.76	-0.3159	-0.0686	-0.2803	-0.0805
2.95	-0.2353	-0.0311	-0.1612	-0.0376
3.15	-0.1336	-0.0071	-0.0827	-0.0142
3.35	-0.0575	0.0014	-0.0301	-0.0013
3.54	-0.0208	0.0030	-0.0076	0.0011
3.74	-0.0022	0.0000	0.0000	0.0000
3.94	0.0000	—	—	—

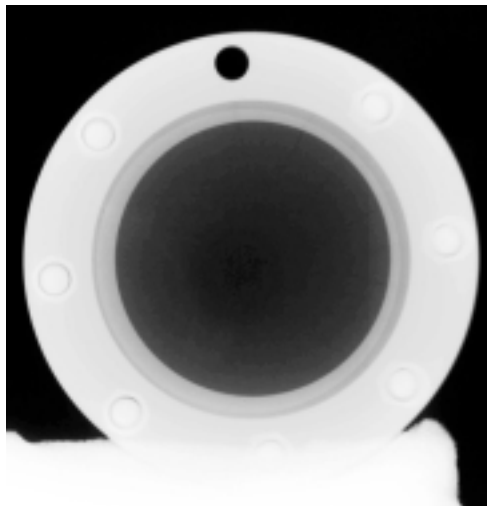


Figure A-10. Target K8-2178 radiograph. Contrast does not show evidence of radial cracking, but does display density gradients.

Table A-14. Quenched target K8-2300 dent data. Impact occurred 0.4375-in. to the right and 0.50-in. high of center at 48.0 ± 1.1 m/s. The average measured dent depth on the cover plate was 10.44 ± 0.03 mm.

Distance (inches)	Center Left-to-right (inches)	Center Top-to-bottom (inches)	Impact Left-to-right (inches)	Impact Top-to-bottom (inches)
0.00	0.0000	0.0000	0.0000	0.0000
0.20	-0.0136	0.0067	-0.0126	0.0074
0.39	-0.0392	0.0134	-0.0403	0.0134
0.59	-0.0992	0.0181	-0.1024	0.0188
0.79	-0.1823	0.0207	-0.2035	0.0103
0.98	-0.2694	0.0179	-0.3062	-0.0268
1.18	-0.3195	0.0036	-0.3778	-0.0863
1.38	-0.3411	-0.0342	-0.4119	-0.1829
1.57	-0.3426	-0.0845	-0.4106	-0.2944
1.77	-0.3057	-0.2008	-0.3817	-0.3540
1.97	-0.2603	-0.2547	-0.3233	-0.3925
2.17	-0.1824	-0.3000	-0.2624	-0.4101
2.36	-0.0739	-0.3173	-0.1761	-0.3966
2.56	-0.0210	-0.3041	-0.0917	-0.3472
2.76	0.0104	-0.2629	-0.0278	-0.2917
2.95	0.0188	-0.1962	-0.0025	-0.1893
3.15	0.0187	-0.1156	0.0094	-0.0903
3.35	0.0122	-0.0509	0.0088	-0.0439
3.54	0.0071	-0.0172	0.0061	-0.0139
3.74	0.0000	0.0000	0.0000	0.0000

Table A-15. Quenched target K8-2180 dent data. Impact occurred 0.125-in. right of center, and on center top-to-bottom at 51.8 ± 1.2 m/s. The average dent depth on the cover plate was 11.88 ± 0.01 mm.

Distance (inches)	Center Left-to-right (inches)	Center Top-to-bottom (inches)	Impact Left-to-right (inches)	Impact Top-to-bottom (inches)
0.00	0.0000	0.0000	0.0000	0.0000
0.20	0.0098	0.0129	0.0058	0.0129
0.39	0.0120	0.0214	0.0046	0.0214
0.59	0.0008	0.0228	-0.0227	0.0228
0.79	-0.0264	0.0108	-0.0919	0.0108
0.98	-0.0972	-0.0328	-0.2331	-0.0328
1.18	-0.1944	-0.0943	-0.3643	-0.0943
1.38	-0.2937	-0.1824	-0.4361	-0.1824
1.57	-0.3749	-0.3159	-0.4678	-0.3159
1.77	-0.4236	-0.3860	-0.4430	-0.3860
1.97	-0.4259	-0.4345	-0.3812	-0.4345
2.17	-0.4071	-0.4676	-0.2919	-0.4676
2.36	-0.3613	-0.4576	-0.1977	-0.4576
2.56	-0.2501	-0.4137	-0.1089	-0.4137
2.76	-0.1198	-0.3497	-0.0366	-0.3497
2.95	-0.0396	-0.2248	-0.0063	-0.2248
3.15	-0.0008	-0.1268	0.0034	-0.1268
3.35	0.0065	-0.0464	0.0052	-0.0464
3.54	0.0047	-0.0119	0.0000	-0.0119
3.74	0.0000	0.0000	—	—

Table A-16. Target K8-2183, inside surface, dent data. Data was only obtained for the impact point. The center point did not have any measurable deformation. Impact occurred 0.5-in. left, and 0.125-in. high of center, at 53.0 ± 1.2 m/s. The average measured dent depth on the inside surface of the holder was 0.15 ± 0.01 mm.

Distance (inches)	Impact Left-to-right (inches)	Impact Top-to-bottom (inches)
0.00	0.0000	0.0000
0.20	-0.0005	-0.0005
0.39	-0.0005	-0.0010
0.59	-0.0010	-0.0010
0.79	-0.0010	-0.0015
0.98	-0.0025	-0.0025
1.18	-0.0035	-0.0040
1.38	-0.0045	-0.0045
1.57	-0.0040	-0.0040
1.77	-0.0050	-0.0060
1.97	-0.0045	-0.0050
2.17	-0.0055	-0.0050
2.36	-0.0060	-0.0060
2.56	-0.0025	-0.0045
2.76	-0.0030	-0.0030
2.95	-0.0030	-0.0025
3.15	-0.0025	-0.0025
3.35	-0.0025	-0.0020
3.54	-0.0015	-0.0015
3.74	-0.0010	-0.0015
3.94	-0.0010	-0.0010
4.13	-0.0005	-0.0005
4.33	-0.0005	-0.0005
4.53	0.0000	0.0000
4.72	0.0000	0.0000

Table A-17. Target K8-2176, inside surface, dent data. Impact occurred 0.125-in. right, and 0.125-in. high of center at 54.3 ± 1.2 m/s. The average measured dent depth on the inside surface of the holder was 1.51 ± 0.08 mm.

Distance (inches)	Center Left-to-right (inches)	Center Top-to-bottom (inches)	Impact Left-to-right (inches)	Impact Top-to-bottom (inches)
0.00	0.0000	0.0000	0.0000	0.0000
0.20	-0.0037	-0.0076	-0.0043	-0.0058
0.39	-0.0089	-0.0112	-0.0116	-0.0117
0.59	-0.0156	-0.0178	-0.0159	-0.0175
0.79	-0.0208	-0.0219	-0.0232	-0.0239
0.98	-0.0290	-0.0285	-0.0300	-0.0292
1.18	-0.0336	-0.0351	-0.0358	-0.0351
1.38	-0.0383	-0.0417	-0.0436	-0.0434
1.57	-0.0455	-0.0473	-0.0529	-0.0473
1.77	-0.0507	-0.0509	-0.0567	-0.0506
1.97	-0.0534	-0.0555	-0.0600	-0.0555
2.17	-0.0561	-0.0576	-0.0617	-0.0573
2.36	-0.0578	-0.0593	-0.0605	-0.0572
2.56	-0.0570	-0.0574	-0.0578	-0.0555
2.76	-0.0547	-0.0545	-0.0536	-0.0514
2.95	-0.0514	-0.0501	-0.0479	-0.0472
3.15	-0.0461	-0.0462	-0.0427	-0.0426
3.35	-0.0398	-0.0413	-0.0370	-0.0364
3.54	-0.0344	-0.0359	-0.0298	-0.0313
3.74	-0.0266	-0.0275	-0.0236	-0.0246
3.94	-0.0248	-0.0211	-0.0174	-0.0180
4.13	-0.0175	-0.0157	-0.0117	-0.0128
4.33	-0.0062	-0.0098	0.0000	-0.0062
4.53	-0.0004	-0.0049	—	0.0000
4.72	0.0059	0.0000	—	—

Table A-18. Target K8-2297, inside surface, dent data. Data was only obtained for the center point. Impact occurred 0.125-in. right, and 0.125-in. high of center, at 54.4 ± 1.3 m/s. The average measured dent depth on the inside surface of the holder was 0.27 ± 0.17 mm.

Distance (inches)	Center Left-to-right (inches)	Center Top-to-bottom (inches)	Impact Left-to-right (inches)	Impact Top-to-bottom (inches)
0.00	0.0000	0.0000	0.0000	0.0000
0.20	-0.0003	0.0024	-0.0005	-0.0004
0.39	-0.0007	0.0018	-0.0010	-0.0009
0.59	-0.0010	0.0013	-0.0009	-0.0013
0.79	-0.0018	0.0007	-0.0019	-0.0018
0.98	-0.0021	-0.0004	-0.0029	-0.0022
1.18	-0.0030	-0.0005	-0.0034	-0.0026
1.38	-0.0038	-0.0025	-0.0038	-0.0041
1.57	-0.0046	-0.0021	-0.0043	-0.0045
1.77	-0.0049	-0.0027	-0.0053	-0.0050
1.97	-0.0058	-0.0038	-0.0058	-0.0054
2.17	-0.0061	-0.0038	-0.0047	-0.0053
2.36	-0.0059	-0.0044	-0.0042	-0.0048
2.56	-0.0053	-0.0035	-0.0052	-0.0052
2.76	-0.0046	-0.0041	-0.0052	-0.0057
2.95	-0.0054	-0.0062	-0.0042	-0.0051
3.15	-0.0052	-0.0097	-0.0036	-0.0045
3.35	-0.0051	-0.0103	-0.0031	-0.0045
3.54	-0.0039	-0.0134	-0.0031	-0.0034
3.74	-0.0032	-0.0140	-0.0031	-0.0024
3.94	-0.0020	-0.0155	-0.0005	-0.0018
4.13	-0.0014	-0.0136	0.0000	-0.0012
4.33	-0.0012	-0.0012	0.0000	-0.0012
4.53	0.0000	-0.0008	—	-0.0001
4.72	0.0002	-0.0028	—	-0.0001
4.92	0.0003	-0.0014	—	—
5.12	0.0000	0.0000	—	—

Table A-19. Target K8-2303, inside surface, dent data. Data was only obtained for the impact point because impact on center, at 55.1 ± 1.3 m/s. The average measured dent depth on the inside surface of the holder was 0.30 ± 0.01 mm.

Distance (inches)	Impact Left-to-right (inches)	Impact Top-to-bottom (inches)
0.00	0.0000	0.0000
0.20	-0.0010	-0.0019
0.39	-0.0041	-0.0039
0.59	-0.0046	-0.0063
0.79	-0.0061	-0.0078
0.98	-0.0076	-0.0102
1.18	-0.0092	-0.0111
1.38	-0.0102	-0.0111
1.57	-0.0107	-0.0120
1.77	-0.0117	-0.0120
1.97	-0.0118	-0.0119
2.17	-0.0113	-0.0109
2.36	-0.0103	-0.0098
2.56	-0.0073	-0.0082
2.76	-0.0069	-0.0057
2.95	-0.0044	-0.0031
3.15	-0.0029	-0.0016
3.35	-0.0009	0.0000
3.54	0.0000	—
3.74	0.0000	—

Table A-20. Target K8-2306, inside surface, dent data. Data was only obtained for the impact point. Impact occurred on center left-to-right, and 0.25-in. high of center at 103.0 ± 2.4 m/s. The average measured dent depth on the inside surface of the holder was 6.09 ± 0.11 mm.

Distance (inches)	Impact Left-to-right (inches)	Impact Top-to-bottom (inches)
0.00	0.0000	0.0000
0.20	-0.0271	-0.0290
0.39	-0.0532	-0.0520
0.59	-0.0749	-0.0766
0.79	-0.0980	-0.1031
0.98	-0.1291	-0.1281
1.18	-0.1547	-0.1561
1.38	-0.1798	-0.1802
1.57	-0.1994	-0.2132
1.77	-0.2261	-0.2367
1.97	-0.2427	-0.2362
2.17	-0.2388	-0.2253
2.36	-0.2109	-0.1868
2.56	-0.1900	-0.1598
2.76	-0.1697	-0.1358
2.95	-0.1463	-0.1139
3.15	-0.1229	-0.0919
3.35	-0.1035	-0.0669
3.54	-0.0761	-0.0409
3.74	-0.0543	-0.0165
3.94	-0.0259	0.0000
4.13	0.0000	—

Target strain gauge data

One to two strain gauges were mounted on center of the target's rear surface to record the deformation relative to the time of impact. If two strain gauges were used, they were oriented with their elements at right angles relative to each other. MicroMeasurements EA-06-500BH-120 strain gauges amplified with Vishay model 2311 signal conditioners were used for this purpose. Several iterations of gauge and lead wire mounting schemes were used to increase data collection time. The gauges and lead wires typically survived after the projectile impact and rebound. Data loss occurred when the gauges were either crushed between the back plate and the rear mounting block or when the cables were destroyed.

The data for the 10 baseline and 8 aged targets are shown in Figures A-11–A-14. An examination of the gauge records provides additional insight regarding the reaction behavior. The back plate strain gauge records show a strong consistency in the impact-induced reaction sequence. The explosive initially behaves as an elastic-solid, transmitting force to the back plate. Near 2000 microstrain at the back plate, the explosive starts to crush and flow radially. The force levels off and then starts to decrease as the explosive crushes until the annular gap is filled and the pressure on the crushed explosive begins to increase again. A comparison of the data also shows a trend toward larger strains and faster reaction

times as the projectile impact velocity is increased and that the delay, ranging from approximately 200 μs to approximately 400 μs , between impact to violent reaction decreases as the projectile velocity increases.

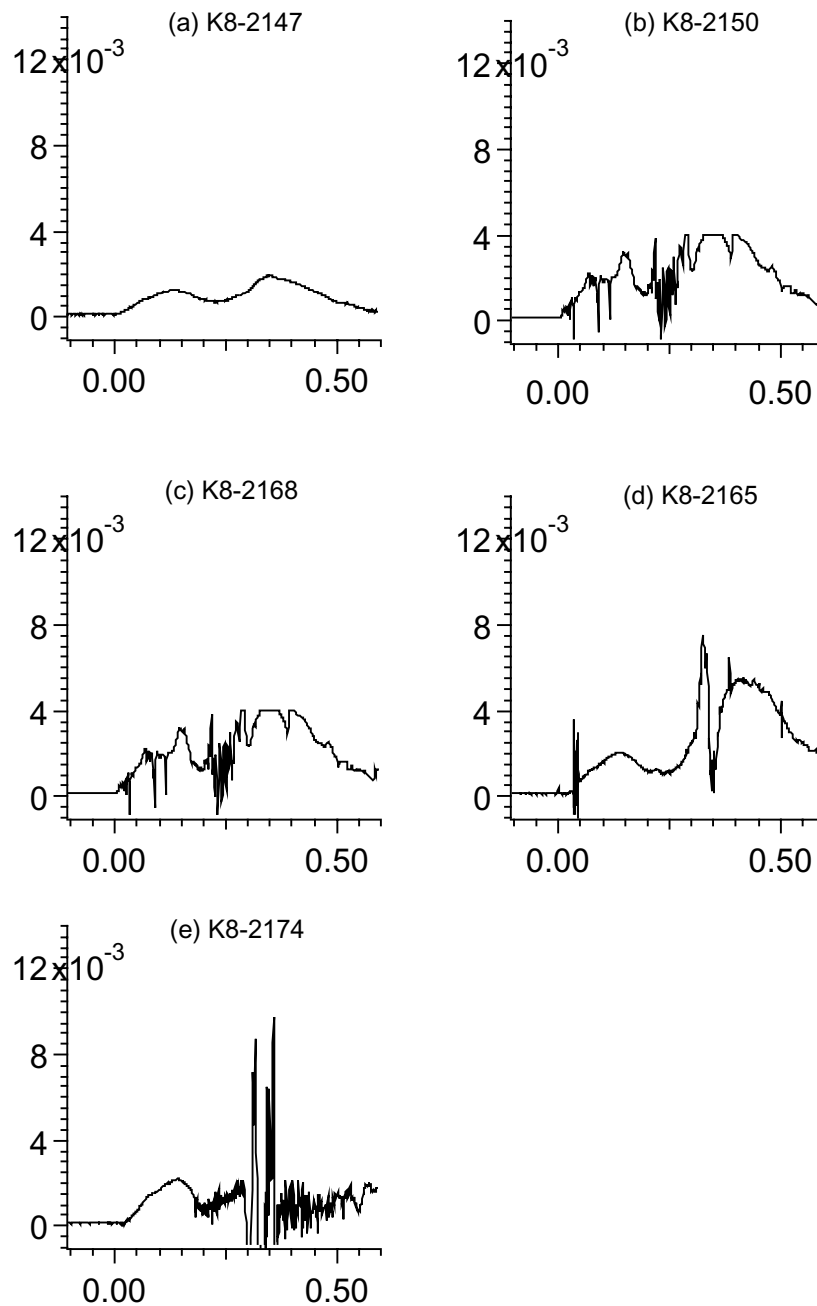


Figure A-11(a-e). Single strain gauge records for the baseline, small, thin targets that resulted in quenched and damaged targets. Strain is plotted as a function of time (ms) after impact in all figures.

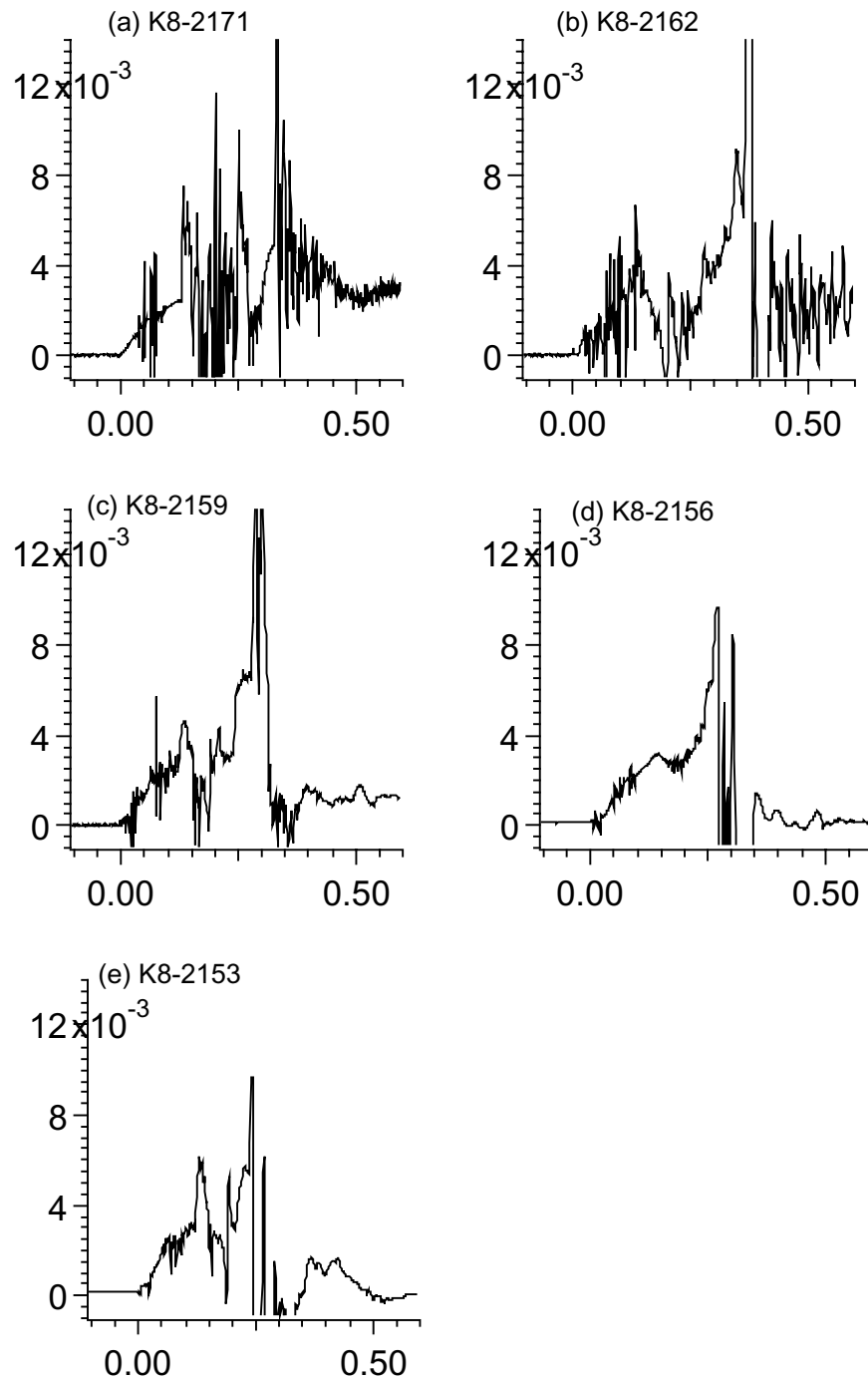


Figure A-12(a-e). Single strain gauge records for the baseline, small, thin targets that reacted violently. Strain is plotted as a function of time (ms) after impact.

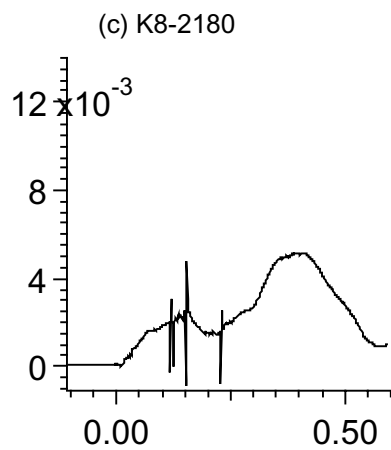
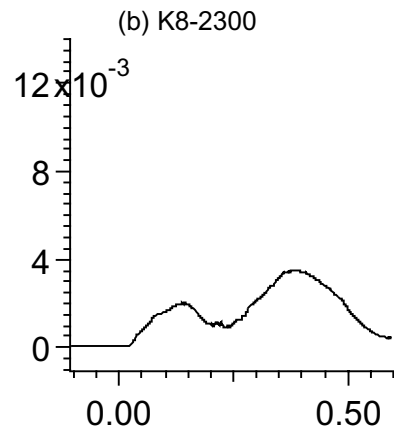
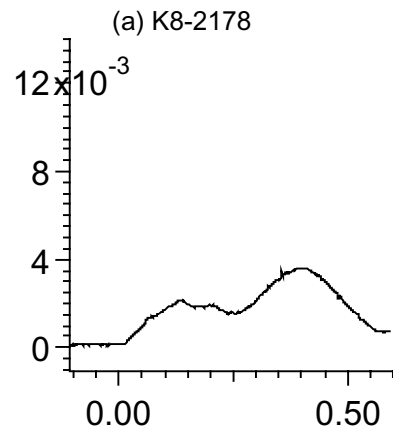


Figure A-13(a-c). Single strain gauge records for the aged, small, thin targets that resulted in quenched and damaged targets. Strain is plotted as a function of time (ms) after impact.

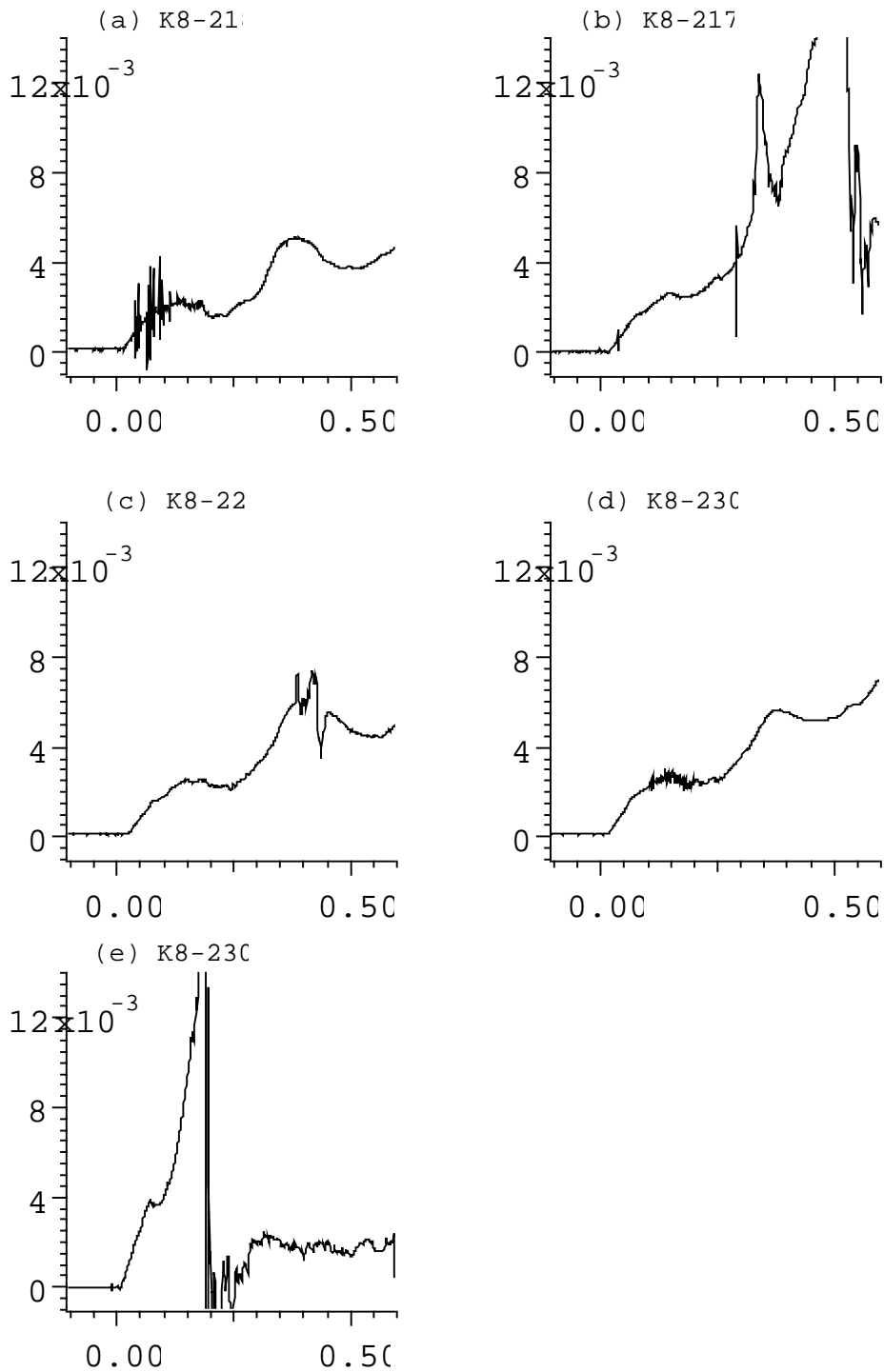


Figure A-14(a-e). Single strain gauge records for the aged, small, thin targets that reacted violently. Strain is plotted as a function of time (ms) after impact.

Enhanced radiographic images of the quenched, damaged targets

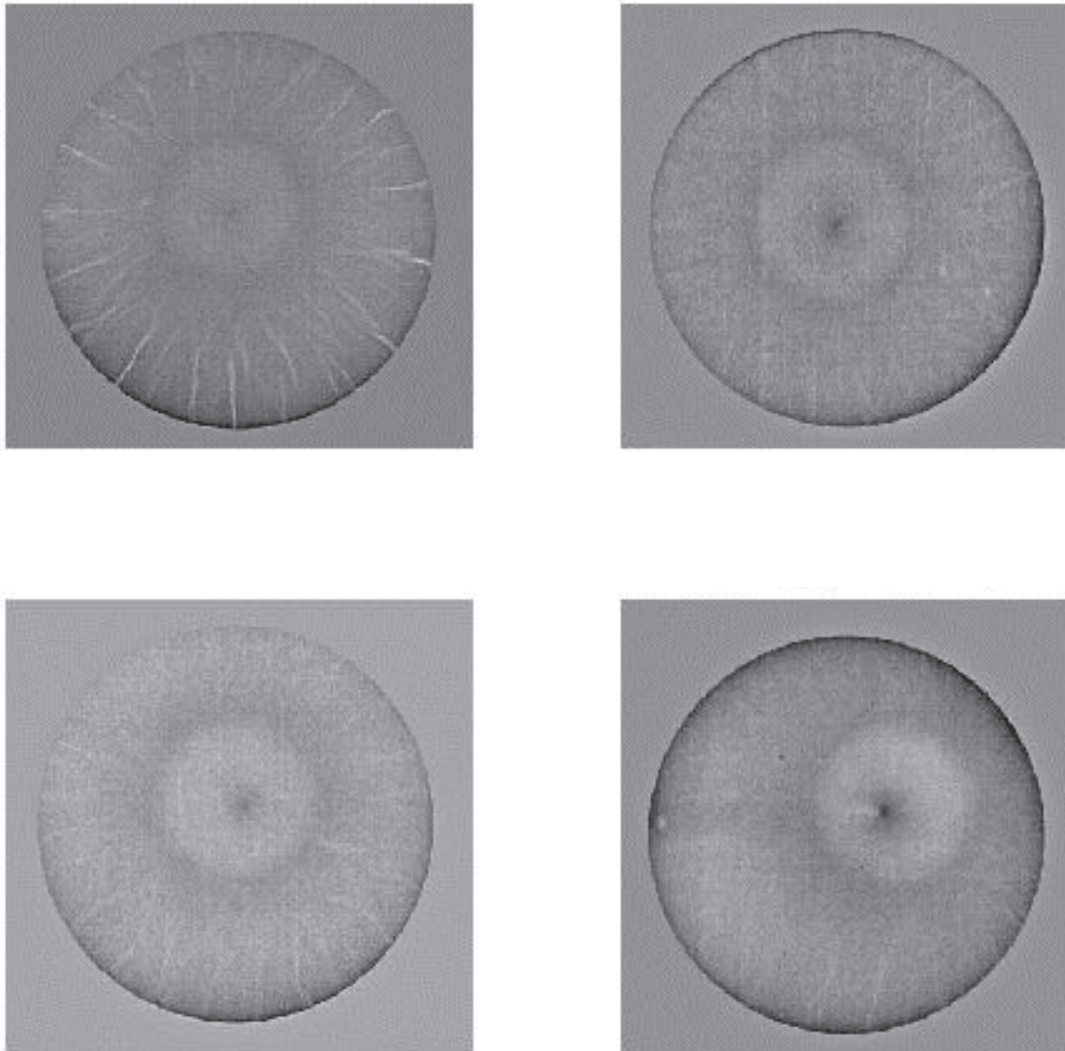
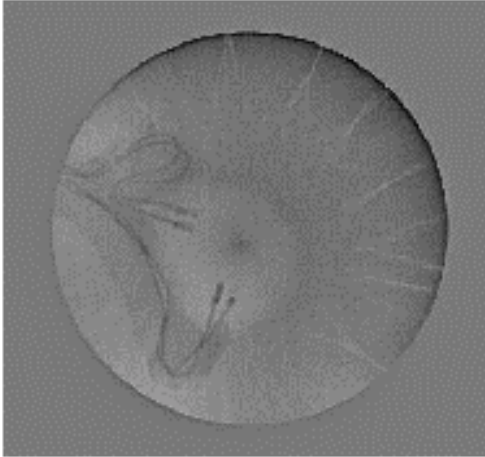
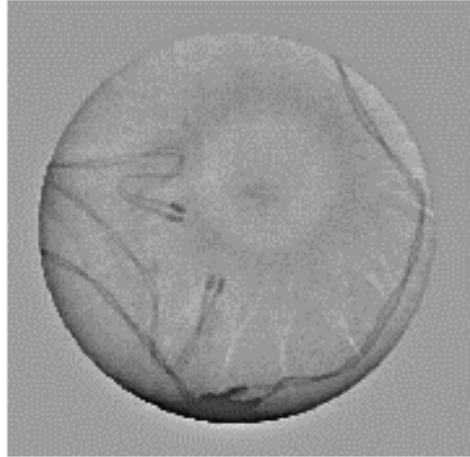


Figure A-15(a-d). Numerically enhanced digital radiographic images of four of the five quenched, damaged baseline targets. The dark center of the impact point is an artifact of the enhancement technique. The data suggest a decrease in the residual crack width as the projectile velocity is increased.

(a) K8-2179, 45.0 m/s,
0.25-in. low, 0.375-in. left



(b) K8-2300, 48.0 m/s,
0.4375-in. right, 0.5-in. high



(c) K8-2180, 51.8 m/s,
0.125-in. right

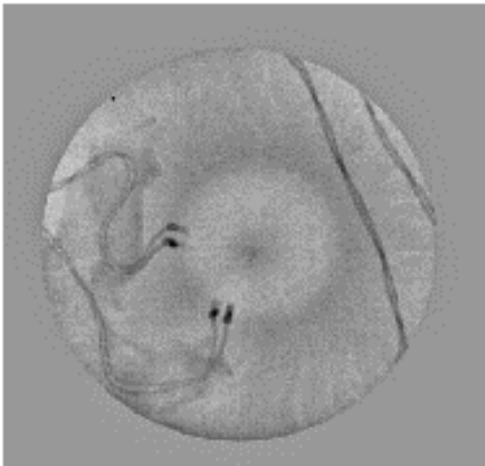


Figure A-16 (a–c). Numerically enhanced digital radiographic images of the three quenched, damaged aged targets. The dark center of the impact point is an artifact of the enhancement technique. The strain gauge leads and solder joints are also evident on the images. No apparent trend in the crack widths is evident as a function of projectile velocity.

This report has been reproduced directly from the best available copy. It is available electronically on the Web (<http://www.doe.gov/bridge>).

Copies are available for sale to U.S. Department of Energy employees and contractors from—

Office of Scientific and Technical Information
P.O. Box 62
Oak Ridge, TN 37831
(423) 576-8401

Copies are available for sale to the public from—

National Technical Information Service
U.S. Department of Commerce
5285 Port Royal Road
Springfield, VA 22616
(800) 553-6847

